This article has been accepted for publication in a future issue of this journal, but has not been fully edited. Content may change prior to final publication. Citation information: DOI 10.1109/TUFFC.2021.3084898, IEEE Transactions on Ultrasonics, Ferroelectrics, and Frequency Control

Feasibility of Model-Assisted Probability of Detection Principles for Structural Health Monitoring Systems based on Guided Waves for Fibre-Reinforced Composites

1st Kilian Tschöke
Systems for Condition Monitoring
Fraunhofer Institute for Ceramic Technologies and Systems IKTS
Dresden, Germany
kilian.tschoeke@ikts.fraunhofer.de

2nd Inka Mueller
Institute of Mechanics
Bochum University of Applied Sciences
Bochum, Germany
inka.mueller@hs-bochum.de

3rd Vittorio Memmolo
Department of Industrial Engineering
Università degli Studi di Napoli Federico II
Naples, Italy
vittorio.memmolo@unina.it

4th Maria Moix-Bonet
Institute of Composite Structures and Adaptive Systems
German Aerospace Center
Braunschweig, Germany
maria.moix-bonet@dlr.de

5th Jochen Moll
Terahertz Photonics
Goethe University of Frankfurt am Main
Frankfurt am Main, Germany
moll@physik.uni-frankfurt.de

6th Yevgeniya Lugovtsova
Acoustic and Electromagnetic Methods Division
Bundesanstalt für Materialforschung und -prüfung (BAM)
Berlin, Germany
yevgeniya.lugovtsova@bam.de

7th Mikhail Golub
Institute for Mathematics, Mechanics and Informatics
Kuban State University
Krasnodar, Russia
m_golub@inbox.ru

8th Ramanan Sridaran Venkat
Non-Destructive Testing & Quality Assurance
Saarland University
Saarbrücken, Germany
ramanan.sridaran@uni-saarland.de

9th Lars Schubert
Systems for Condition Monitoring
Fraunhofer Institute for Ceramic Technologies and Systems IKTS
Dresden, Germany
lars.schubert@ikts.fraunhofer.de

***Abstract*—In many industrial sectors, Structural Health Monitoring (SHM) is considered as an addition to Non-Destructive Testing (NDT) that can reduce maintenance effort during lifetime of a technical facility, structural component or vehicle. A large number of SHM methods is based on ultrasonic waves, whose properties change depending on structural health. However, the wide application of SHM systems is limited due to the lack of suitable methods to assess their reliability. The evaluation of the system performance usually refers to the determination of the Probability of Detection (POD) of a test procedure. Up to now, only few limited methods exist to evaluate the POD of SHM systems, which prevent them from being standardised and widely accepted in industry. The biggest hurdle concerning the POD calculation is the large amount of samples needed. A POD analysis requires data from numerous identical structures with integrated SHM systems. Each structure is then damaged at different locations and with various degrees of severity. All of this is connected to high costs. Therefore, one possible way to tackle this problem is to perform computer-aided investigations. In this work, the POD assessment procedure established in NDT according to the Berens model is adapted to guided wave-based SHM systems. The approach implemented here is based on solely computer-aided investigations. After efficient modelling of wave propagation phenomena across an automotive component made of a carbon fibre-reinforced composite, the POD curves are extracted. Finally, the novel concept of a POD map is introduced to look into the effect of damage position on system reliability.**

***Index Terms*—Acousto Ultrasonics, Reliability Assessment, Damage Detection, Automotive Industry, Elastodynamic Finite Integration Technique**

This article has been accepted for publication in a future issue of this journal, but has not been fully edited. Content may change prior to final publication. Citation information: DOI 10.1109/TUFFC.2021.3084898, IEEE Transactions on Ultrasonics, Ferroelectrics, and Frequency Control

I. Introduction to Guided Wave-Based Structural Health Monitoring

In the field of Structural Health Monitoring (SHM) an enormous amount of work, research and development has been carried out for several decades. SHM is very attractive for many industry sectors, *e. g.* aerospace, automotive and nuclear, allowing to increase safety and reduce operative costs by introducing a change in the maintenance philosophy. Nevertheless, there is still a gap between scientific research and the industrial deployment of various SHM methods. A main challenge for a broad application of SHM systems is the lack of suitable methods to assess their performance [1], [2], [3].

SHM systems are based on different physical principles adopted to detect the presence of a damage. Examples are modal analysis, electromechanical impedance measurement, measurement of static parameters (strain measurement), methods of acoustic emission analysis, or methods based on elastic waves [4]. In particular, SHM methods based on elastic waves have been developed for a variety of industrial sectors. The focus of the present work is on Ultrasonic Guided Waves (UGW), which are a special form of elastic waves guided by the boundaries of structures like plates, pipes, *etc.* They are particularly suitable for damage detection because they are affected by the media they are travelling through and are able to interact even with small hidden flaws, moreover, allowing the inspection of inaccessible areas. Methods based on UGW are widely used and specific approaches have been developed to detect various types of damage, such as delamination, holes, cracks, notches, corrosion or the degradation of welded and riveted joints. A comprehensive summary and a basic description of these methods can be found in [5].

A schematic drawing of a guided wave based SHM system on a plate-like structure is shown in Figure 1. In the context of this explanatory example, W1 to W4 are piezoelectric transducers (PZT) attached to the structure. These transducers are able to emit and to receive elastic waves in the ultrasonic frequency range (20 kHz to 1 GHz). If a transducer emits such a signal, it is called actuator; if it records, it is called sensor or receiver. SHM methods based on ultrasonic signals actively excited by actuators are called Acousto Ultrasonic (AU) methods in the literature [6], [7]. They are further differentiated into those exploiting Pitch-Catch or Pulse-Echo measurements [8]. In the former the actuator and sensor are different PZTs and the focus is on the wave transmission through the damage, whereas the latter exploits the same transducer to excite and sense UGW focusing the attention on the flaw induced reflections. This work focuses on guided wave based SHM systems using a Pitch-Catch configuration and a frequency of 225 kHz to detect damages in a composite structure. Over the years, many studies have shown the potential of guided waves to detect and localise damage in fibre composite structures proving their suitability for SHM of aerospace and automotive components [6], [9], [10], [11], [12], [13].

A known method to evaluate the performance of SHM systems consists in the determination of the Probability of Detection (POD) of a test method. In general, the POD can be understood as a probability curve, obtained by experiments or by simulations, which indicates the probability with which a fault can be detected [15]. The POD is usually a function of the size of a defect which is represented in POD curves. The regulatory base for SHM is still on its way and with one issue being a lack of POD evaluation methods applicable for the reliability assessment of SHM systems [1]. Therefore, the development of POD methods for SHM systems is urgently required [3]

Since the transducers of an SHM system are permanently installed on a monitoring object, a purely experimental determination of the POD would involve a high experimental effort as well as an enormous amount of material. The need for numerical simulation to investigate and perform reliability assessment of such systems has been already pointed out in the literature [3]. Therefore, efficient and reliable simulation of the UGW propagation and their interaction with damage is a current research topic in the field of SHM [16]. Furthermore, various regulations, such as the SAE ARP 6461[1], pave the way for computer-aided investigation of SHM systems. The reliable simulation of wave propagation phenomena is essential for this. That is why current research continues to deal with the efficient simulation of wave propagation phenomena. So [18] write: "The simulation of wave propagation phenomena - even for linear two-dimensional cases - is still challenging for numerical methods. Particularly in the case of large domains (*e. g.* seismic waves) or short wavelengths (*e. g.* ultrasound), [...]".

The present work focuses on two main challenges regarding the reliability assessment of SHM systems. Firstly, the POD is determined for a guided wave based SHM system using simulated input data for a model-assisted POD. After obtaining the POD curves, the effect of the damage position on the system reliability is analysed using a novel concept: the POD map.

This contribution is structured as follows. The introduction to SHM systems that has just been given is followed in Section II by a description of the concept of the POD as it is used in the field of Non-Destructive Testing (NDT). It is followed by a section that shows why this approach has to be supported by numerical models for SHM systems. Afterwards, Section III shows the governing equations of elastic waves and a selected discretisation method. This method, known as the Elastodynamic Finite Integration Technique (EFIT), is specially adapted for the modelling of structures made of carbon fibre-reinforced composites. The procedure and parameters of the modelling are explained for a selected component from the automotive industry. In Section IV the results of the numerical experiments are presented. Based on these results,

[1] "SAE International is a global association of [...] engineers and related technical experts in the aerospace, automotive and commercial-vehicle industries" [17]. An Aircraft Recommended Practice is a guideline for developments in aircraft industry.

This article has been accepted for publication in a future issue of this journal, but has not been fully edited. Content may change prior to final publication. Citation information: DOI 10.1109/TUFFC.2021.3084898, IEEE Transactions on Ultrasonics, Ferroelectrics, and Frequency Control

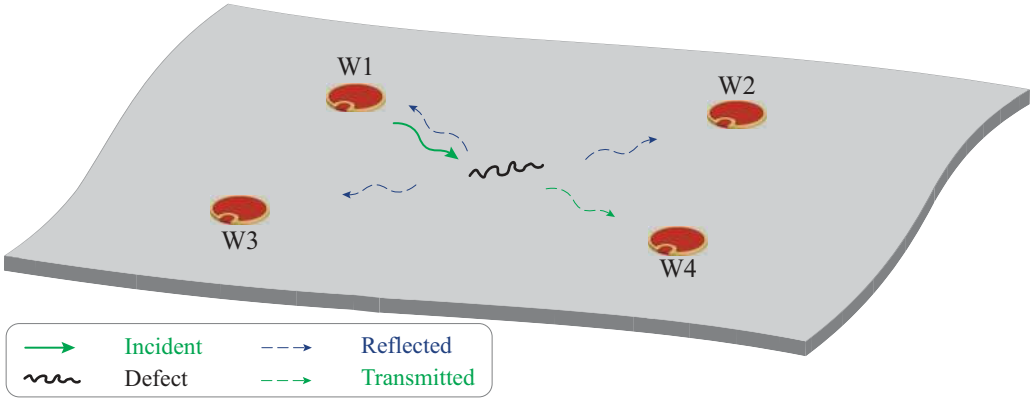

Fig. 1. Schematic drawing of a PZT-based guided waves SHM system on a free plate-like structure according to [14]. The system consists of piezoelectric transducers (W1-W4), which can emit and receive ultrasonic signals. These signals interact with damage and can be partially reflected or transmitted.

a model-assisted concept for determining the POD of a SHM system is presented, which includes the visualisation of system performance with the novel concept of so-called POD maps. The POD maps are finally discussed and the present work concludes with a summary in Section V.

II. Probability of Detection for SHM systems

This section starts with an overview of the available literature in POD, originating from classical NDT methods and continues with the theoretical background for the calculation of the POD curves in SHM systems. Finally, the concept of model-assisted POD is presented.

A. Theory of POD

The POD indicates the probability of a system to detect a specific flaw [19]. The original development and description of the POD come from aviation and were driven by the high safety requirements in this industry. A historical overview can be found in [20]. The standards developed by Berens were used to determine the reliability of NDT methods used in regular inspections. Later it was estimated that approximately 25 % of an aircraft's operating costs are due to inspections and maintenance [9]. Therefore, the use of integrated monitoring methods, *e. g.* based on actively excited UGW, allows for structural evaluation and has a potential of replacing costly inspections.

Testing and monitoring methods must be qualified in accordance with the applicable test regulations to demonstrate a sufficiently high level of reliability in damage detection and assessment. This reliability assessment is based on the POD: a monotonous function of a parameter of interest which characterises the flaw [21], [22]. This parameter is usually the size of the flaw and therefore the POD is often given as a function of it [23]. In addition, critical flaw sizes which affect the integrity of the component during its lifetime are often known from the design. Therefore, a flaw of the critical size must be detected by a test procedure reliably so that the acceptance criterion can be met [24]. From this point, POD curves correlate each flaw size to the probability of detecting that flaw during lifetime by the specified test procedure. The data to populate a POD curve can be obtained either by measurements or by numerical simulations which must include the information about the critical flaw and its size. From these diagrams the $a_{90/95}$ value can be obtained. This value denotes the flaw size which can be detected with a probability of 90 % and a confidence level of 95 % [25]. Practically, this flaw size represents quantitatively the performance of the inspection procedure and the $a_{90/95}$ value is used to characterise the reliability of the system. A test system is considered suitable for the present test task if $a_{90/95}$ is smaller than the acceptance criterion.

Two parametric methods are mainly used to determine a POD in the field of NDT [9], [21], [26]. This is, on the one hand, a method based on binary data, the Hit-Miss Analysis, and, on the other hand, the method of Analysis of the Signal Response. The Berens method which is accepted as a standard can generally be categorised as a method of signal response analysis. The development from the hit-miss analysis through the analysis of the signal response to the Berens method is also described as an "evolution" of the POD calculation [27].

The standard work of POD determination in the field of NDT is the summary of various investigations in the aviation sector of the US Department of Defense, from which a manual on the determination of the reliability of NDT systems was developed [28]. The manual, *MIL-HDBK* for short, and the associated software *mh1823* form an internationally accepted standard for performing POD analyses. The theoretical foundations on which the MIL-HDBK is based can be found in [23] and were later supplemented by [26], [29], [30]. These publications, in turn, form the basis for a large number of other works. A fundamental overview and an introduction to factors influencing POD can be found in [31], [32], [33]. However, a standard for carrying out POD investigations for SHM systems has not been established yet [1], [2], [4], [19], [34].

In the following the Berens method is described and the assumptions are discussed with regard to its application for the reliability assessment of SHM systems. Specifications within this work which are made for the final application

This article has been accepted for publication in a future issue of this journal, but has not been fully edited. Content may change prior to final publication. Citation information: DOI 10.1109/TUFFC.2021.3084898, IEEE Transactions on Ultrasonics, Ferroelectrics, and Frequency Control

example should be regarded as one way of implementation. The decisions made are based on existing research work and are intended to stimulate further scientific discussion.

The variables whose correlation is examined in POD observations are the damage size a and the signal response $\hat{a}$, also called damage index (DI). In the context of UGW, the DI is obtained from measurement signals after processing steps. A characteristic to describe the damage size depends on the application, the test procedure and the type of damage. Possible characteristics are, for example, the flaw length, diameter, depth, area or volume.

The basic assumption of the Berens method is a linear relationship between the damage size a and the damage index $\hat{a}$. Under certain circumstances, this is only given in a semi-logarithmic or double-logarithmic scale, *i. e.* the variables $\log a$ and $\log \hat{a}$ are included [28]. In the following derivation, the notation a and $\hat{a}$ is continued without loss of generality.

Remark II.1 (Selection of a suitable damage index)
Different guided wave modes interact differently with a certain type of damage [6]. Whether there is a linear relationship between damage size and damage index depends in particular on the mode shapes of the stress components relative to the location of a damage. A suitable damage index shall, on the one hand, be adjusted to the type of damage, and on the other hand, it has to be demonstrated that it is linear with the damage size. A selection of possible damage indices is provided by [10], [35]. For anisotropic materials, *e. g.* fibre reinforced composites, [19] show that the damage index

$$DI = 1 - |CC| \ , \tag{1}$$

where CC describes the correlation coefficient, is linearly related to the area of a delamination on a logarithmic scale. The cross CC is determined between the baseline and the current measurement[2]. The authors in [10], [12], [13] examine a large number of DIs regarding their interaction with typical damage in composites. They ultimately identify 4 DIs that are optimally suited for the stated purpose. Among them is also the DI as given in Equation (1). Based on these results from the literature, the damage index based on CC is used in this work.

In general, the relationship between a and $\hat{a}$ can be described according to a linear model

$$Y = X \cdot \beta + \varepsilon \ , \tag{2}$$

whereby the usual notation from statistics is used and with which:

$$Y = \begin{pmatrix} \hat{a}_1 \\ \vdots \\ \hat{a}_n \end{pmatrix}, \quad X = \begin{pmatrix} 1 & a_1 \\ \vdots & \vdots \\ 1 & a_n \end{pmatrix}, \\ \beta = \begin{pmatrix} \beta_0 \\ \beta_1 \end{pmatrix}, \quad \varepsilon = \begin{pmatrix} \varepsilon_1 \\ \vdots \\ \varepsilon_n \end{pmatrix} \ . \tag{3}$$

The vector of the dependent variable Y contains the DIs $\hat{a}_i$ for the associated damage sizes a_i determined after n measurements. The matrix X is called data matrix or design matrix. β denotes the vector of the regression coefficients and ε denotes the error vector, which describes external influences or measurement errors.
In the linear model, the following assumptions are still applied: the error components are independent and $\varepsilon \sim \mathcal{N}(0, \tau^2)$ applies, *i. e.* they are normally distributed with expected value 0 and have the identical variance τ^2. Under these assumptions estimators b and ς^2 for β and τ^2 respectively can be determined according to

$$b = \left(X^T X\right)^{-1} X^T Y \ , \\ \varsigma^2 = \frac{1}{n} \left(Y - Xb\right)^T \left(Y - Xb\right) \ . \tag{4}$$

In general, Berens uses the maximum likelihood method to determine the estimators [23]. Under the above conditions on ε, this coincides with the least squares estimator presented in Equation (4). With the estimator b, the regression line is determined as

$$\hat{a} = b_0 + b_1 a \ . \tag{5}$$

A flaw in the test object is accepted as detected if $\hat{a}$ exceeds a given threshold. This threshold is called decision threshold $\hat{a}_{dec}$. The larger the decision threshold, the larger is the smallest damage size that can be detected.

Remark II.2 (Selection of the decision threshold)
For SHM systems based on UGW, [11] write that "no physical interpretation is available to set a general threshold". The reasons for this are the different wave modes, reflections, mode conversions and anisotropic behaviour, the latter aspect being mainly valid for fibre composites. For real measurements, the decision threshold can be set at a level of 3 dB or 6 dB above the noise level. The noise level can be obtained from measurements of the reference state if multiple and statistically independent measurements are available. For this purpose, the baseline measurement must be repeated several times [14]. Usually, the inherent noise characterising the signal response shows a normal distribution. When considering the specific metric (*i. e.* DI) it is possible to verify the normality assumption with a variety of parametric or non-parametric tests. Among them, the Kolmogorov-Smirnov test is certainly one of the most accepted and can be applied successfully even when a limited number of samples is available, like in [36] where the satisfaction of the Gaussian assumption was achieved. If

[2]In real laboratory measurements, the electronics may cause a phase shift between different time signals. To minimise the influence of this phase shift, the cross correlation coefficient can also be determined by the *Hilbert* transformations of the time signals. Since such a phase shift does not occur in simulations, the DI is determined directly from the time signals in the context of the present work.

This article has been accepted for publication in a future issue of this journal, but has not been fully edited. Content may change prior to final publication. Citation information: DOI 10.1109/TUFFC.2021.3084898, IEEE Transactions on Ultrasonics, Ferroelectrics, and Frequency Control

no noise level is known, as can be the case in simulations, it is possible to choose the decision threshold as the minimum of the regression line or to obtain it from attendant simulations [19]. In the present contribution, noise is inserted into the simulations. This is explained in Section III-B.

Since $\hat{a} \sim \mathcal{N}\left(X\beta, \tau^2\right)$ also

$$\hat{a}_{dec} = \Phi^{-1}\left(0.5, Xb, \varsigma^2\right) \ , \tag{6}$$

applies, where Φ is the distribution function of the standard normal distribution. The $POD(a)$ for the damage size a is defined according to

$$POD(a) = 1 - \Phi\left(\frac{\hat{a}_{dec} - (b_0 + b_1\, a)}{\varsigma}\right) \ . \tag{7}$$

Alternatively and according to [14], with the definition of

$$\mu_{POD} = \frac{\hat{a}_{dec} - b_0}{b_1}, \qquad \tau_{POD} = \frac{\varsigma}{b_1} \tag{8}$$

Equation (7) is rewritten as

$$POD(a) = \Phi\left(\frac{a - \mu_{POD}}{\tau_{POD}}\right) \ . \tag{9}$$

That is, a given damage size a generates a DI $\hat{a}$ and the $POD(a)$ is the probability that $\hat{a}$ exceeds the threshold $\hat{a}_{dec}$:

$$POD(a) = P(\hat{a} > \hat{a}_{dec}) \ . \tag{10}$$

The damage size for which $POD(a_{90}) = 0.9$ applies is denoted by a_{90} [26].

Since the determined POD curve is obtained from a specific sample, the real function can vary around the fitted curve. For this reason it is necessary to determine confidence bands around the POD curve in which the real function lies with the highest possible confidence level [15]. There are different approaches on the kind of confidence such as tolerance bands, prediction bands and confidence bands, which all return the degree of probability, belief, or support that an unknown parameter value lies in a specific interval. However, among those interval estimators, the latter one is the most commonly adopted. Although the amount of data available in model-assisted POD is countless and does not suggest the use of this approach. Practical POD estimations are almost always made from data of limited sample sizes, and hence require confidence bounds to be given [37], motivating its use even in this context. There are various approaches in the literature for determining the confidence bands [15], [24], [27]. A comparison of different methods can be found in [38]. The derivation according to Berens can be found in [23], [28]. The final resulting value $a_{90/95}$ specifies the flaw size a which can be detected by measuring the DI $\hat{a}$ with a probability of 90 % and a confidence level of 95 % [14].

B. Model-assisted POD (MAPOD)

Influencing parameters that have been considered so far and implemented in models within the framework of the determination of a POD for classical NDT methods are the "human factor", the test conditions or environmental conditions, the test equipment (sensitivity, resolution), the test process, the material under investigation or interactions between all the factors mentioned [33]. According to the conclusions emerging from sixth European American Workshop on Reliability of NDE [39], influences can be broken down into four groups:

(i) intrinsic capability,
(ii) environmental parameter,
(iii) human factors, and
(iv) organisational factors.

However, influencing factors differ between NDT and SHM methods. For example, the "human factors" can be neglected when using an SHM system [40]. Furthermore, the limitation of environmental conditions with regard to integrated systems is not expedient, since they should also be used in operation, *i. e.* under fluctuating environmental parameters. Environmental conditions, material properties and the geometry of the objects under investigation can be identified as the cause for fluctuations in monitoring systems [2]. For SHM systems, the installation of the actuators and sensors on a structure and the distribution of the damage are further factors influencing the variations in damage detection [4]. The measurement results of an SHM system are usually closely related to the structure on which it is applied and therefore cannot be transferred to other structures [27]. The latter authors also consider the variability of damage, *i. e.* its position and orientation, as parameters influencing the POD of an SHM system. Furthermore, the probability of damage occurring and its distribution are often unknown in reality [27].

In summary, the verification of the POD for SHM systems requires not only a variation of failure types and sizes as well as the geometry and structure of various coupons and components, but also the consideration of various environmental parameters. The effort and scope for tests to prove a POD is considerably greater for SHM systems compared to NDT methods and cannot be achieved by laboratory tests alone. As [19] write: "Due to the fixed mounting of SHM systems on structures, experimentally based investigation is particularly difficult and resource consuming". Investigations of the POD must therefore also be carried out based on simulations, also known as Model Assisted POD (MAPOD). In the literature, MAPOD approaches are basically divided into two categories [2], [22], [41], [27]:

1) **Transfer function method**: Empirically determined POD curves are used to obtain estimates of the POD of a comparable inspection scenario. This means that empirical data from several individual experiments are combined to form an overall statement about the POD of a NDT method. During the determination of the new POD curve, it is argued how significant factors influence the POD. The influencing factors represent well-understood physical phenomena.
2) **Completely model-based**: With this approach, factors that cause fluctuations within an inspection are systematically modelled and their effects identified. The models are used to estimate signal responses and fluctuations.

This article has been accepted for publication in a future issue of this journal, but has not been fully edited. Content may change prior to final publication. Citation information: DOI 10.1109/TUFFC.2021.3084898, IEEE Transactions on Ultrasonics, Ferroelectrics, and Frequency Control

Current research is initially concerned with the development and understanding of the POD concept in the context of SHM, since there is no standard procedure for determining the POD of an SHM system [27]. The present work follows a completely model-based approach.

III. Numerical Modelling

In the present work, the Elastodynamic Finite Integration Technique (EFIT) is used for modelling the wave propagation phenomena through an automotive component made of composite material. The EFIT method allows to model the complete wave field in homogeneous and heterogeneous, isotropic and anisotropic materials. Further details can be found in [42], [43], [44], [45]. The following section lays the groundwork for the wave field modelling based on the EFIT and applies the method to the current test object.

A. Modelling of UGW in anisotropic materials

The Cauchy's equation of motion describe the propagation of elastic waves in an (inhomogeneous) medium:

$$\rho \frac{\partial^2}{\partial t^2} u = \nabla \cdot \sigma + f \ , \tag{11}$$

with $\rho = \rho(x_1, x_2, x_3)$ being the mass density, $u = (u_1, u_2, u_3)$ the displacement vector, t the time, $\sigma = \{\sigma_{ij}\}_{i,j=1,2,3}$ the stress tensor and $f = (f_1, f_2, f_3)$ the body forces, respectively. In the case of linear deformations, Hooke's law holds true

$$\sigma = C \cdot \eta \ , \tag{12}$$

where η denotes the strain

$$\eta = \frac{1}{2}\left(\nabla u + (\nabla u)^{\mathrm{T}}\right) \tag{13}$$

and

$$C = \begin{pmatrix} C_{11} & C_{12} & C_{13} & C_{14} & C_{15} & C_{16} \\ & C_{22} & C_{23} & C_{24} & C_{25} & C_{26} \\ & & C_{33} & C_{34} & C_{35} & C_{36} \\ & & & C_{44} & C_{45} & C_{46} \\ & \text{symm.} & & & C_{55} & C_{56} \\ & & & & & C_{66} \end{pmatrix} \tag{14}$$

is the elasticity matrix for the case of anisotropic materials.

The basic idea of the EFIT is to perform an integration of the differential equations over a defined control volume. First, equations (11) and (12) are transformed into a first order hyperbolic system by introducing the particle velocity $v = \frac{\partial}{\partial t} u$:

$$\rho \frac{\partial}{\partial t} v = \nabla \cdot \sigma + f \ , \tag{15}$$

and

$$\frac{\partial}{\partial t} \sigma = C \cdot \frac{\partial}{\partial t} \eta \ . \tag{16}$$

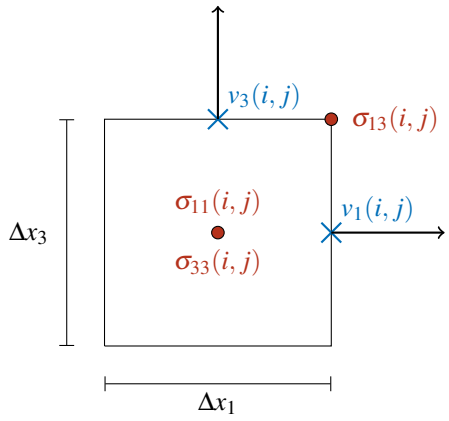

Fig. 2. The staggered grid cell i, j of the 2D-EFIT scheme.

For readability, we present the method only for the two-dimensional case in the $x_1 - x_3-$plane and for the first component v_1 of (15). The exemplary equation is

$$\rho \frac{\partial}{\partial t} v_1 = \frac{\partial}{\partial x_1}\sigma_{11} + \frac{\partial}{\partial x_3}\sigma_{13} + f_1 \ . \tag{17}$$

The integral form of (17) over such a control volume V reads

$$\int_V \rho \frac{\partial}{\partial t} v_1 \ dV = \int_V \left(\frac{\partial}{\partial x_1}\sigma_{11} + \frac{\partial}{\partial x_3}\sigma_{13} + f_1\right) \ dV \ . \tag{18}$$

With the help of the divergence theorem, we transfer (18) into

$$\int_V \rho \frac{\partial}{\partial t} v_1 \ dV = \int_V \left(\frac{\partial}{\partial x_1}\sigma_{11} + \frac{\partial}{\partial x_3}\sigma_{13} + f_1\right) \ dV \tag{19}$$

$$= \int_S (\sigma_{11}, \sigma_{13}) \cdot n \ dS + \int_V f_1 \ dV \ , \tag{20}$$

where n is the outer unit normal vector of the boundary S. The most commonly used grid cells are Cartesian ones and there are different possibilities to locate the unknowns within the control volume. Figure 2 shows the staggered case often used for elastodynamic problems. Assuming the staggered spatial grid and applying the midpoint rule to the cell i, j we obtain a quadrature scheme from (19) which reads

$$\begin{aligned} \rho \frac{\partial}{\partial t} v_1(i,j) \cdot \Delta x_1 \Delta x_3 = &(\sigma_{11}(i+1,j) - \sigma_{11}(i,j)) \cdot \Delta x_3 \\ &+ (\sigma_{13}(i,j) - \sigma_{13}(i,j-1)) \cdot \Delta x_1 \\ &+ f_1(i,j) \cdot \Delta x_1 \Delta x_3 \end{aligned} \tag{21}$$

Dividing (21) by $\Delta x_1 \Delta x_3$ results in

$$\begin{aligned} \rho \frac{\partial}{\partial t} v_1(i,j) = &\frac{\sigma_{11}(i+1,j) - \sigma_{11}(i,j)}{\Delta x_1} \\ &+ \frac{\sigma_{13}(i,j) - \sigma_{13}(i,j-1)}{\Delta x_3} + f_1(i,j) \ . \end{aligned} \tag{22}$$

For time integration, the Leap frog scheme is chosen to

This article has been accepted for publication in a future issue of this journal, but has not been fully edited. Content may change prior to final publication. Citation information: DOI 10.1109/TUFFC.2021.3084898, IEEE Transactions on Ultrasonics, Ferroelectrics, and Frequency Control

complete the EFIT procedure as follows

$$v_1^{n+\frac{1}{2}}(i,j) = v_1^{n-\frac{1}{2}}(i,j) + \frac{\Delta t}{\rho \Delta x_1}\left(\sigma_{11}^n(i+1,j) - \sigma_{11}^n(i,j)\right) + \frac{\Delta t}{\rho \Delta x_3}\left(\sigma_{13}^n(i,j) - \sigma_{13}^n(i,j-1)\right) + \frac{\Delta t}{\rho} f_1^n(i,j)\ . \quad (23)$$

Here upper index in v_1 and σ_{1k} corresponds to discretization in time domain with time step Δt. The remaining equations of (15) and (16) are discretized employing almost the same procedure.

As boundary conditions a stress-free boundary is assumed. This boundary condition is implemented with the help of the stress-imaging method. This technique is attributed to [46] and is described in detail in [47], [48] for staggered grids.

B. Properties and parameters of the sample application

In the present work, test objects made of a carbon fibre reinforced plastic (CFRP) material are considered. The models are the result of work from the project *CarbonSafe*. The aim of this project was the development of a suitable SHM system for safety-relevant components made of CFRP in the automotive industry. More results of the project can be found in [49], [50], [51].

Modelling of the multi-layered structure made of an anisotropic composite material is possible by EFIT if the elastodynamic material parameters of a single layer are known. Using a three-dimensional discretization of the structure, each ply can then be modelled as one or more material cells in thickness direction. Since the single layers are usually thinner than 500 µm, the corresponding cells have a very small dimension in the thickness direction. To satisfy the stability condition of explicit time integration *i. e.* the Courant-Friedrichs-Lewy condition (CFL), the time step of the overall algorithm becomes extremely small, which leads to a considerable computing time expenditure, especially when the number of layers increases. Although this approach would ensure high fidelity modelling of the structural behaviour under transient dynamic load, the computational effort can be insufficient if the laminated plate has a certain number of plies. To reduce computational effort significantly, the multi-layered material can be idealised by the Equivalent Single Layer (ESL) approach. This method has already been successfully used to model SHM systems based on UGW for composites [34]. In particular, it ensures a good computational efficiency without reducing the model performance. At the same time, it offers high accuracy in modelling of the global structure of the wave field [52] and returns reasonable indication about the interaction between wave and through thickness damage [34]. Originally, the ESL approach was developed and used for fatigue tests supported by Finite Element Modelling on composite materials and is particularly suitable for thin laminate structures [53]. The aim of the method is to obtain a single layer, whose stiffness is equivalent to that of the multi-layered material. The equivalent structure is obtained by computing the effective stiffness matrix using classical lamination theory, first order shear deformation theory or other plate theories. They are derived by making suitable assumptions on the displacement of plate particles according to the shear behaviour of the structure. Basic assumptions are:

- Each individual layer is linearly elastic.
- The laminate is very thin, *i. e.* the thickness is much smaller than the other dimensions.
- The thickness is constant.
- Due to the thin laminate, the plane stress condition holds true.

Another general condition for the validity of simplified plate theories concerns the wavelength which shall be significantly greater than the structure thickness. This is usually the case for UGW whose wavelength is in the range of a several tens of millimetres propagating in plate-like laminates of a few millimetres of thickness. Further explanations regarding plate theories and the propagation of Lamb waves in laminates can be found in [54]. Moreover, a detailed derivation of the effective stiffness matrix can be found in [55].

If the elastodynamic constants of a single layer and the stacking sequence of the laminate are known, the effective stiffness matrix can be calculated with the freely usable program *eLamX*^{2}, which is developed at the TU Dresden at the Institute of Aerospace Engineering. The program and an online manual describing the basic operation of *eLamX*^{2} can be obtained from [56].

The automotive component made of CFRP is shown in Figure 3. A CAD data set of the geometry of the component was provided by the partner in the *CarbonSafe* project, which was used to extract the curvilinear edge of the component as a polygon. For the shown test specimen, the multi-layered structure is given with the layup of [0/45/90/0/-45/90], whose equivalent elastic matrix is

$$C_{ESL} = \begin{pmatrix} 89.1 & 18.1 & 18.1 & 0 & 0 & 0 \\ 18.1 & 89.1 & 18.1 & 0 & 0 & 0 \\ 18.1 & 18.1 & 89.1 & 0 & 0 & 0 \\ 0 & 0 & 0 & 20.7 & 0 & 0 \\ 0 & 0 & 0 & 0 & 20.7 & 0 \\ 0 & 0 & 0 & 0 & 0 & 20.7 \end{pmatrix} \text{GPa}\ . \quad (24)$$

Figure 3 also shows a schematic drawing of the 2D model of the test specimen including the coordinate system. A total of four piezoelectric circular transducers were applied to the structure. Their centers are located at the positions

W1: $x_1 = 80$ mm, $x_3 = 80$ mm,
W2: $x_1 = 240$ mm, $x_3 = 80$ mm,
W3: $x_1 = 150$ mm, $x_3 = 180$ mm,
W4: $x_1 = 300$ mm, $x_3 = 260$ mm .

In the ESL method, a damage within the structure can be modelled as a local stiffness reduction. The damage idealisation in a CFRP structure using the ESL method has already been described and investigated in the literature [57]. The

This article has been accepted for publication in a future issue of this journal, but has not been fully edited. Content may change prior to final publication. Citation information: DOI 10.1109/TUFFC.2021.3084898, IEEE Transactions on Ultrasonics, Ferroelectrics, and Frequency Control

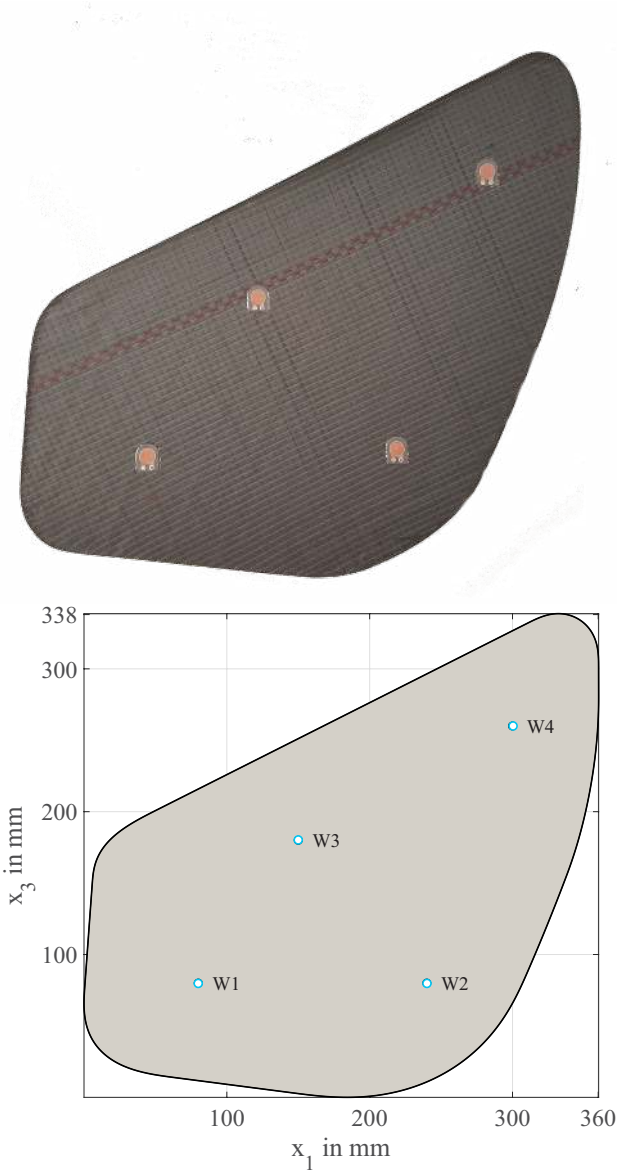

Fig. 3. Top: Picture of an automotive component made of CFRP. Bottom: Schematic drawing of the 2D model of the test specimen including marked positions of the piezoelectric transducers (•).

degradation of the composite material can be modelled by reducing its stiffness according to

$$\tilde{C} = \kappa \cdot C \ , \tag{25}$$

where $\kappa = 0.5$ is the so called scaling factor [57]. This assumption is supported by [58]. Impact damages lead to micro-cracks in fibre composites and these lead to a local reduction of stiffness. A corresponding approach within the framework of the ESL method was confirmed in [34] by experimental NDT measurements on a damaged test specimen.

In the present work, the configuration of a damage is varied, *i. e.* one damage is repeatedly introduced at one position and changed in form and orientation, leading to introduction of variation, as it is necessary for the POD analysis. In general, impact induced damage in composite materials can be assumed to be elliptical [19]. As part of the final reports of the SARISTU[3] project, different papers showed investigations on impact damage to structures made of composite materials in aircraft industry [10], [11]. The authors specify delaminations with a radius of more than 20 mm as critical because they lead to exterior damage barely visible by visual inspection. For the automotive sector, the publication of a corresponding specification is not known to the authors of the present paper. Therefore, a delamination area of 100 mm^2 is considered critical for the automotive CFRP component used in this study. This size is specified as the acceptance criterion for later examination.

The entire area to be discretized, which encloses the above-mentioned specimen from the *CarbonSafe* project, has an extension of 361 mm × 339 mm (Figure 4). The number of grid cells was 722 × 678 cells, resulting in $\Delta x = 0.5$ mm. Damage was modelled at 27 different locations shown in Figure 4 in separate simulation runs. Each damage was modelled as a local change in stiffness according to Equation (25) with $\kappa = 0.5$. The damage size a is the area A in mm^2. Starting from a given area, a damage was assumed to be elliptical with the semi-axes p and q. The semi-axes were randomly varied five times per given area A. A total of 11 different areas were specified for each damage position, from 50 mm^2 to 150 mm^2 with an increase of 10 mm^2. First the semi-axis p was determined, the length of which was normally distributed. The radius of a circle with identical area A was assumed as the expected value μ. The standard deviation is defined by the equation

$$\tau = \frac{\mu - 3\Delta x}{3} \ . \tag{26}$$

Varying of damage orientation includes a variation of specific importance for the performance assessment based on the POD. With this specification, 99.73 % of the values for p are in the interval $\mu \pm 3\tau$ and p is at least $3\Delta x$ long, *i. e.* it can be represented in the grid of discretization. From the value for p and $A = \pi pq$, q was finally determined. This procedure basically follows the investigations of [27] which consider the variability of a damage as an influencing parameter on the POD of a SHM system. Other sources of variation such as influence of environmental and operational conditions like stress, temperature, *etc.* have not been taken into account in this purely simulation-based approach.

The transducers were modelled as a point source whereas an actuator acted as surface forces f_1 and f_3 in both spatial directions, respectively. A five-cycle Hanning-windowed cosine pulse with a centre frequency of 225 kHz was chosen as the excitation signal. For comparable structures and components, a damage interaction potential has already been shown in this frequency interval [49]. The observation time was set to 150 µs, which results in a total of 3600 time steps according to the CFL-condition.

[3]Smart Intelligent Aircraft Structures [59].

This article has been accepted for publication in a future issue of this journal, but has not been fully edited. Content may change prior to final publication. Citation information: DOI 10.1109/TUFFC.2021.3084898, IEEE Transactions on Ultrasonics, Ferroelectrics, and Frequency Control

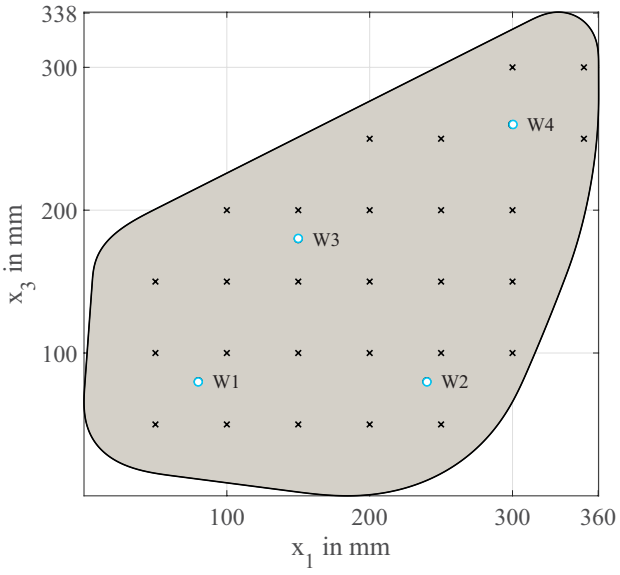

Fig. 4. Schematic drawing of the selected damage positions (×) as well as the positions of the piezoelectric transducers (•) in the test specimen.

IV. Results and Discussion

This chapter evaluates the performance of the formerly described guided wave based SHM system by means of POD and is organised as follows. The wave field model, upon which the POD evaluation is based, is presented in Section IV-A. In Section IV-B, the POD curves for single combinations of actuator-sensor pairs and damage locations are determined. Section IV-C presents the POD maps as a method to display the POD evaluation for all damage locations. Lastly, Section IV-D combines the POD maps to obtain the performance evaluation of the complete SHM system and analyses the effect of the damage position on the system reliability.

A. Description of the wave field

Figure 5 shows exemplary wave fields of the absolute value of the displacement in the test specimen at $t = 15\,\mu s$ and at $t = 30\,\mu s$, left and right figures, respectively. The transducer W1 was the actuator in this case. The baseline, the damage case with inserted damage with $A = 100\,mm^2$, $p = 6.11\,mm$ and $q = 5.2\,mm$ at the position $x_1 = 100\,mm$ and $x_3 = 100\,mm$ as well as the difference signal of the two mentioned states are presented in Figure 5. In the representations of the baseline and the damage case, the expected directional dependence of the wave field due to the anisotropy of the material is observed. The interaction with the damage can be seen more clearly when the difference signal is shown. The damaged area acts as a scatterer and in addition it can be seen how the scattered part of the wave also propagates directionally from the position $x_1 = 100\,mm$ and $x_3 = 100\,mm$. These results correspond to the results of laser vibrometer measurements on comparable CFRP structures [6], [7].

B. POD evaluation

To evaluate the POD of the SHM system, all transducers were used sequentially as actuators and the other three transducers as sensors. According to the Pitch-Catch approach, the transducer that is used as an actuator is not simultaneously adopted as sensor. The DI in Equation (1) is chosen to represent the signal response $\hat{a}$. In the literature, a linear relationship was shown for DI with the area of a damage in anisotropic materials on double logarithmic axes [19].

The entire evaluation algorithm consists in determining the time signals of the baseline and the damage state at each sensor for each damage position, for each damage size a, for each damage configuration and for each actuator-sensor combination. This results in a total number of 5940 simulations. From the time signals, the damage index $\hat{a}$ is calculated.

The decision threshold $\hat{a}_{dec}$ was obtained from the data of the simulations. The procedure was based on the method presented in [19]. The basic idea is that only the DIs on indirect paths are evaluated to determine the decision threshold. Thus, only the DIs that are dominated by reflection components of the time signals are considered. For each damage position, the most distant Pitch-Catch path between two transducers was first determined. By the distance between a path and the damage position, the Euclidean distance between the location of the damage and the perpendicular foot on the path is meant. For this path, the DIs $\hat{a}$ were then determined for both actuator-sensor combinations for the 5 modelled damage sizes with $a = 50\,mm^2$ according to (1). This resulted in a total distribution of 270 $\hat{a}$ values (Figure 6). From this distribution, the 90 % percentile was chosen as the decision threshold. The evaluation of the time signals of the u_1 component resulted in $\hat{a}_{dec}$=0.0109 and for the u_3 component in $\hat{a}_{dec}$=0.0087. Based on these values, it can be assumed that the u_3 component is generally more sensitive and that considering the u_3 component will result in smaller values for a_{90} and $a_{90/95}$. However, later analysis shows that such a conclusion cannot be derived from the numeric value of the decision threshold.

The regression line between the damage size a and the DI $\hat{a}$ was then determined for each actuator-sensor combination. The POD curves according to Berens' model were then determined using the above mentioned specifications. Within the scope of the evaluation algorithm, two POD curves were generated for each damage position and each actuator-sensor combination. One based on the time signals of the u_1 component and one based on the time signals of the u_3 component. An example of the described evaluations is shown in Figures 7 and 8. The following evaluations refer to the case of a damage at the position $x_1 = 100\,mm$ and $x_3 = 100\,mm$. Figure 7 shows the determined regression line between $\hat{a}$ and a based on the time signals of the u_1 component for the actuator-sensor combination W1-W2. Since the damage position in this case is close to the actuator W1 (Figure 3), it can be expected that the influence on the time signals is relatively high, *i. e.* even very small damage should be detectable. Nevertheless, there are also a few outliers in Figure 7, which can be related

This article has been accepted for publication in a future issue of this journal, but has not been fully edited. Content may change prior to final publication. Citation information: DOI 10.1109/TUFFC.2021.3084898, IEEE Transactions on Ultrasonics, Ferroelectrics, and Frequency Control

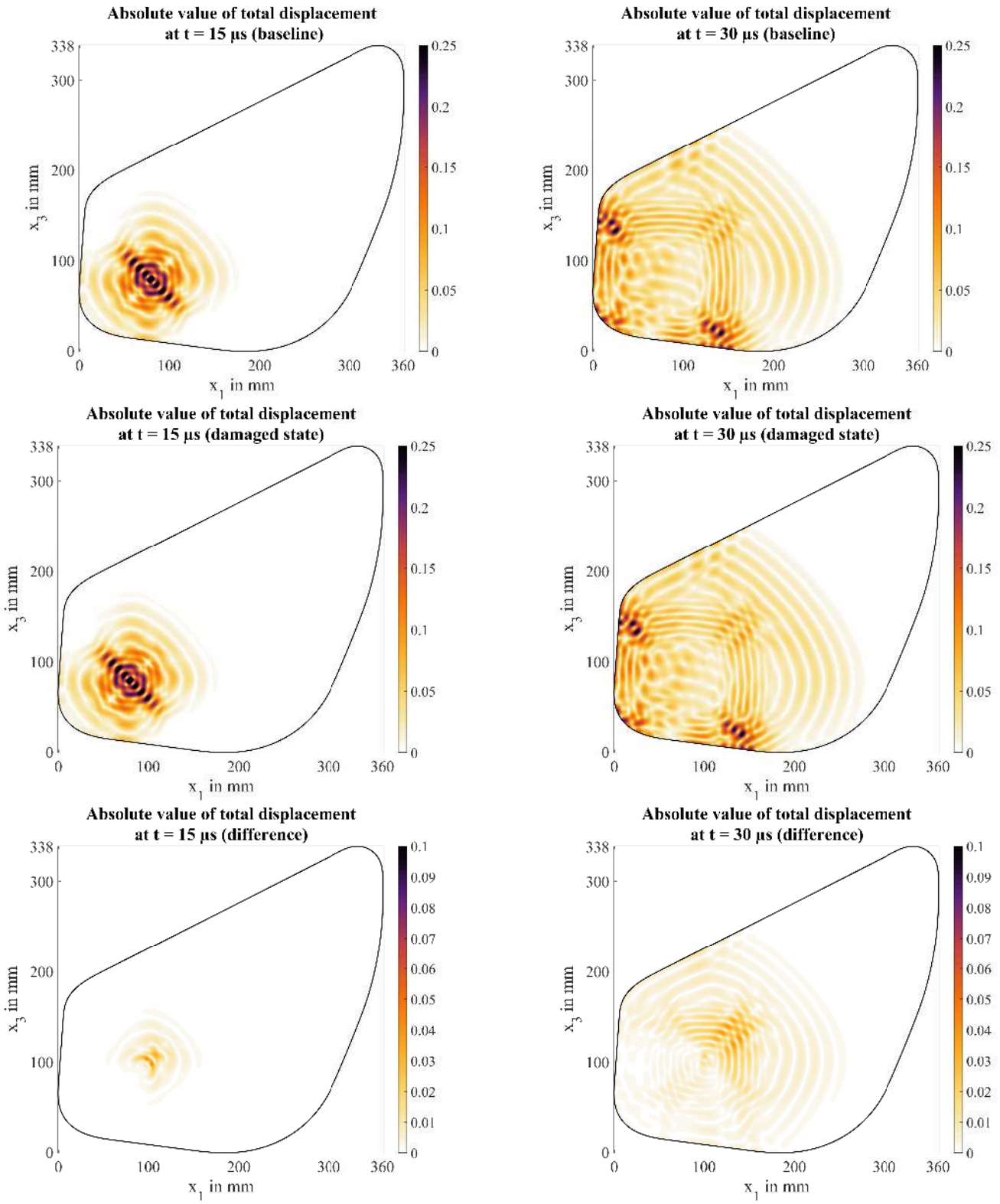

Fig. 5. Absolute value of the total displacement in the test specimen. The left and right columns show the wave fields at $t = 15\,\mu s$ and $t = 30\,\mu s$, respectively. The upper row shows the baseline, the middle row the damaged state with the damage introduced with $A = 100\,mm^2$, $p = 6.11\,mm$ and $q = 5.2\,mm$ at the position $x_1 = 100\,mm$ and $x_3 = 100\,mm$. The bottom line shows the differential signal of the two states mentioned. The transducer W1 was the actuator.

This article has been accepted for publication in a future issue of this journal, but has not been fully edited. Content may change prior to final publication. Citation information: DOI 10.1109/TUFFC.2021.3084898, IEEE Transactions on Ultrasonics, Ferroelectrics, and Frequency Control

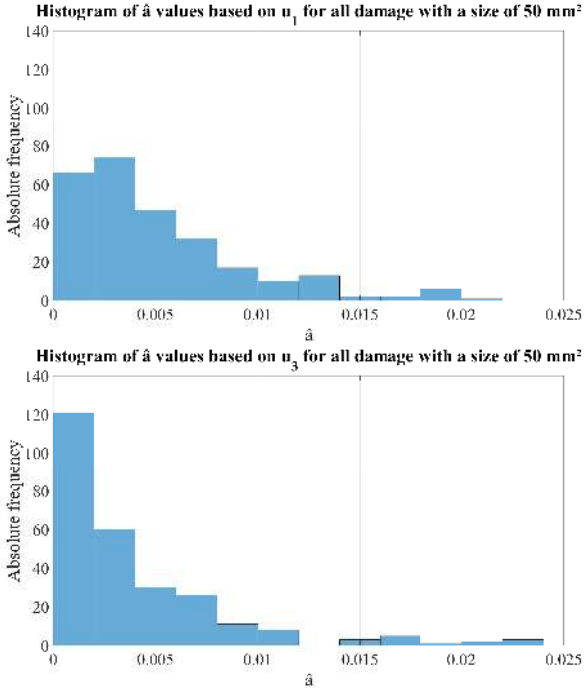

Fig. 6. Histograms of $\hat{a}$ values determined for the most distant Pitch-Catch paths for all damage positions and for the smallest damage size of 50 mm^2. Above: When evaluating u_1. Below: When evaluating u_3.

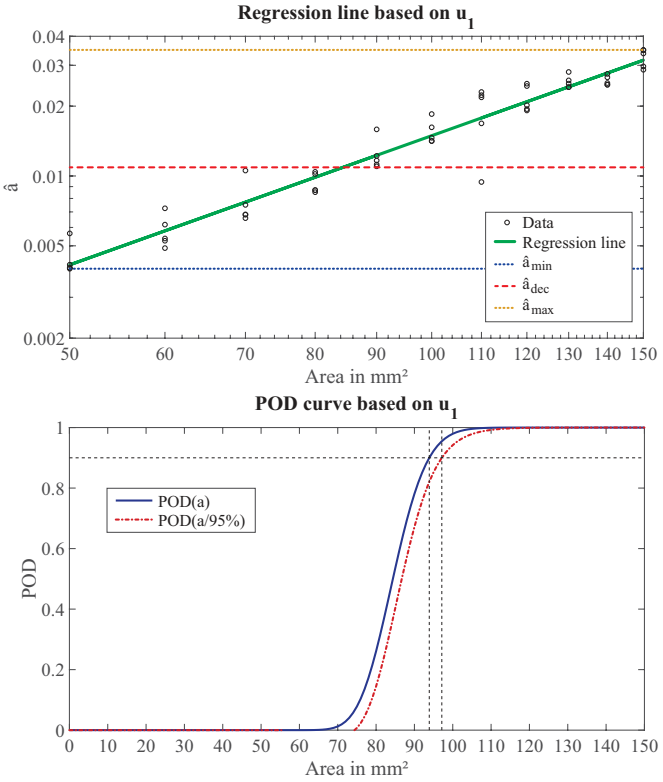

Fig. 7. Top: Representation of the linear relationship between $\hat{a}$ and a including regression line and parameters of the investigation when evaluating the u_1 time signals. The transducer W1 was the actuator, the transducer W2 the sensor. The damage was located at the position $x_1 = 100$ mm and $x_3 = 100$ mm. Bottom: Representation of the determined POD curve of a damage at the position $x_1 = 100$ mm and $x_3 = 100$ mm when evaluating the u_1 time signals. The values $a_{90} = 93.87$ mm^2 and $a_{90/95} = 97.14$ mm^2 were determined.

to the modelling of the damages. When defining the ellipses, one of the semi-axes was assumed to be normally distributed and the second semi-axis was calculated from the area of the damage. The normal distribution of the semi-axes resulted in very narrow ellipses in a few cases. These ellipses, depending on the orientation between the damage and the wave front, can lead to less or more interaction for the same size of damage.

During the evaluation the minimum and maximum of the $\hat{a}$ values were determined as $\hat{a}_{min} = 0.0040$ and $\hat{a}_{max} = 0.0349$, respectively. The resulting POD curve is also shown in Figure 7, from which $a_{90} = 93.87\,\text{mm}^2$ and $a_{90/95} = 97.14\,\text{mm}^2$ were obtained. If the time signals of the u_3 component are evaluated, comparable values result with $a_{90} = 106\,\text{mm}^2$ and $a_{90/95} = 109.18\,\text{mm}^2$. Nevertheless, in this example the u_1 component is more sensitive, *i. e.* more suitable for detecting the damage as one can see from the smaller values of a_{90} and $a_{90/95}$.

From the estimated POD, it is possible to obtain a_{90} for the defect size detectable with a 90 % probability, which is standard accepted as safe. Taking into account the confidence interval, $a_{90/95}$ is obtained as the minimal defect size detectable with a 90 % probability with a 95 % confidence. This means that the defect size detected in 90 % of cases has a 95 % probability to be smaller than $a_{90/95}$. Many publications allude to the $a_{90/95}$ criteria for reliability, which is the flaw size at which POD is 90 % with a confidence of 95 % or greater. Although the $a_{90/95}$ has been criticized for its arbitrariness, it is the de-facto metric for quantifying the performance of the system (the detectability criterion) giving that it represents the minimum detectable damage with a statistically meaningful belief. Nonetheless, for the sake of clarity, both a_{90} and $a_{90/95}$ are discussed afterwards.

If, in contrast, the actuator-sensor combination W3-W4 is evaluated for the above-mentioned damage position, the dependence of the POD on the location of the damage or on the arrangement of the transducers within the system becomes apparent. The damage position is no longer on a direct Pitch-Catch path between W3 and W4 (Figure 3). The difference signal at W4 is not dominated by the transmitted wave components, but by those scattered from the damaged area. It is therefore to be expected that larger values for a_{90} and $a_{90/95}$ will be retrieved for this actuator-sensor combination. Corresponding results based on the evaluation of the u_1 component are shown in Figure 8. A smaller slope of the regression line compared to that in Figure 7 can be observed. As parameters $\hat{a}_{min} = 0.0021$ and $\hat{a}_{max} = 0.0160$ were determined. If one compares the maximum $\hat{a}$ value of 0.0160 obtained in this case (W3-W4) with that of the actuator-sensor combination W1-W2 (0.0349), it becomes clear that the same damage sizes can result in different damage indices. From the constructed POD curve $a_{90} = 156.12\,\text{mm}^2$ and $a_{90/95} = 168.56\,\text{mm}^2$ could

This article has been accepted for publication in a future issue of this journal, but has not been fully edited. Content may change prior to final publication. Citation information: DOI 10.1109/TUFFC.2021.3084898, IEEE Transactions on Ultrasonics, Ferroelectrics, and Frequency Control

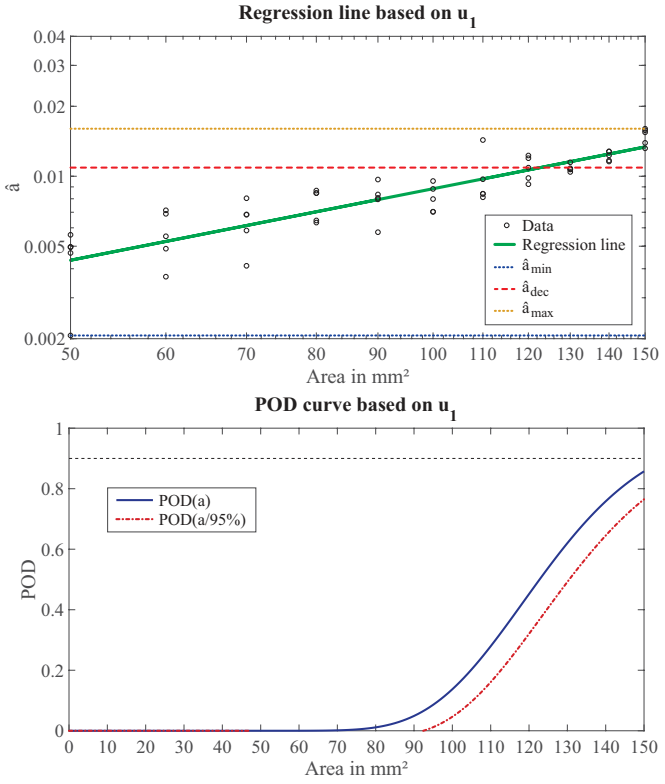

Fig. 8. Top: Representation of the linear relationship between $\hat{a}$ and a including regression line and parameters of the investigation when evaluating the u_1 time signals. The transducer W3 was the actuator, the transducer W4 the sensor. The damage was located at the position $x_1 = 100\,\text{mm}$ and $x_3 = 100\,\text{mm}$. Bottom: Representation of the determined POD curve of a damage at the position $x_1 = 100\,\text{mm}$ and $x_3 = 100\,\text{mm}$ when evaluating the u_1 time signals. The values $a_{90} = 156.12\,\text{mm}^2$ and $a_{90/95} = 168.56\,\text{mm}^2$ were determined.

be determined (bottom in Figure 8). The flatter slope of the POD curve in Figure 8 compared to that in Figure 7 also confirms the preliminary consideration that larger defects must be occur for the actuator-sensor combination W3-W4 than for the combination W1-W2 to obtain a POD of 0.9. However, if the u_3 component is evaluated for the actuator-sensor combination W3-W4, $a_{90} = 50.5\,\text{mm}^2$ and $a_{90/95} = 52.84\,\text{mm}^2$ are obtained. The reflected part of the wave, which influences the difference signal and thus DI, dominates in the case of the u_3 component. This is therefore more suitable for the evaluation of the actuator-sensor combination W3-W4 in order to detect the above-mentioned damage.

It is worth noting that Figure 7 shows a more heterogeneous scatter of data around the predicted value. However, the POD approach is based on certain strict assumptions about the regression model best fitting the data, which is demanded, as such, to accommodate the linear relationship between the signal response and the flaw size while ensuring a limited deviation of the signal response around the estimated value and the same deviation across all values of the flaw size. Nonetheless, the lack of homoscedasticity (homogeneous scattering) showed by some paths in the relationship between the response and flaw size will not alter the generality of the discussion made afterwards and the qualitative validity of the results already shown (*i. e.* inspection be transducer pair W1-W2 will always return a performance much higher than that performed by W3-W4 when damage is locate at $x_1 = 100\,\text{mm}$ and $x_3 = 100\,\text{mm}$). The use of the POD approach is indeed aimed to establish a rigorous way to evaluate how the damage position affects the performance of the system (measured by the path-based $a_{90/95}$) rather than to find out the more plausible $a_{90/95}$ value.

C. Creation of POD maps

It has already been shown in the literature that the POD within an SHM network depends on the damage location [4], [60]. Since the PZTs of an SHM system are permanently installed, the distance between the transducers and a damage varies depending on the location of the damage and thus also the POD. This effect is emphasised in anisotropic materials, since their force-deformation behaviour is directional and thus also the propagation speed of guided wave modes.

The influence of the chosen path between two transducers on the damage detection was investigated in [19]. Using numerical simulations on an anisotropic composite specimen, the authors show that a DI varies depending on the location within an SHM network. The numerical and experimental investigations in [4] also showed that the arrangement of the PZTs has an influence on the damage detection. Since the location, size and orientation of an accidental induced damage are unknown in reality, the best possible arrangement of the transducers is also unknown. However, if the arrangement of the transducers within an SHM network is fixed, it follows that the location, size and orientation of a damage must be varied in order to assess the POD.

For this purpose there is the possibility to create a POD map to investigate the influence of the damage location on the POD of an SHM system. A POD map is created by specifying a fixed number of points on the investigated object where damage is modelled. For each damage location, the size of the damage is varied and the values a_{90} as well as $a_{90/95}$ are determined using the Berens method. This relationship can be visualised in a height profile map. Such maps based on computer-aided investigations of an SHM system were presented in [60], [61].

The POD evaluation described in Section IV-B was then carried out for all damage positions. Figures 9 and 10 show the determined a_{90} and $a_{90/95}$ values for the actuator-sensor-combination W1-W2 when evaluating the u_1 and u_3 time signals, top and bottom, respectively. The damage positions that do not meet the acceptance criterion of $100\,\text{mm}^2$ are marked in black. These representations also confirm the location dependency of the POD within the test specimen. In general, when evaluating the u_1 component, it can be determined that the acceptance criterion can be met in the area between W1, W2 and W3. This is not true in a region in the "Northeast" of the specimen (Figure 9). These damage positions are also not in the transmission path between W1 and W2. The magnitude of the DI is significantly influenced by the

This article has been accepted for publication in a future issue of this journal, but has not been fully edited. Content may change prior to final publication. Citation information: DOI 10.1109/TUFFC.2021.3084898, IEEE Transactions on Ultrasonics, Ferroelectrics, and Frequency Control

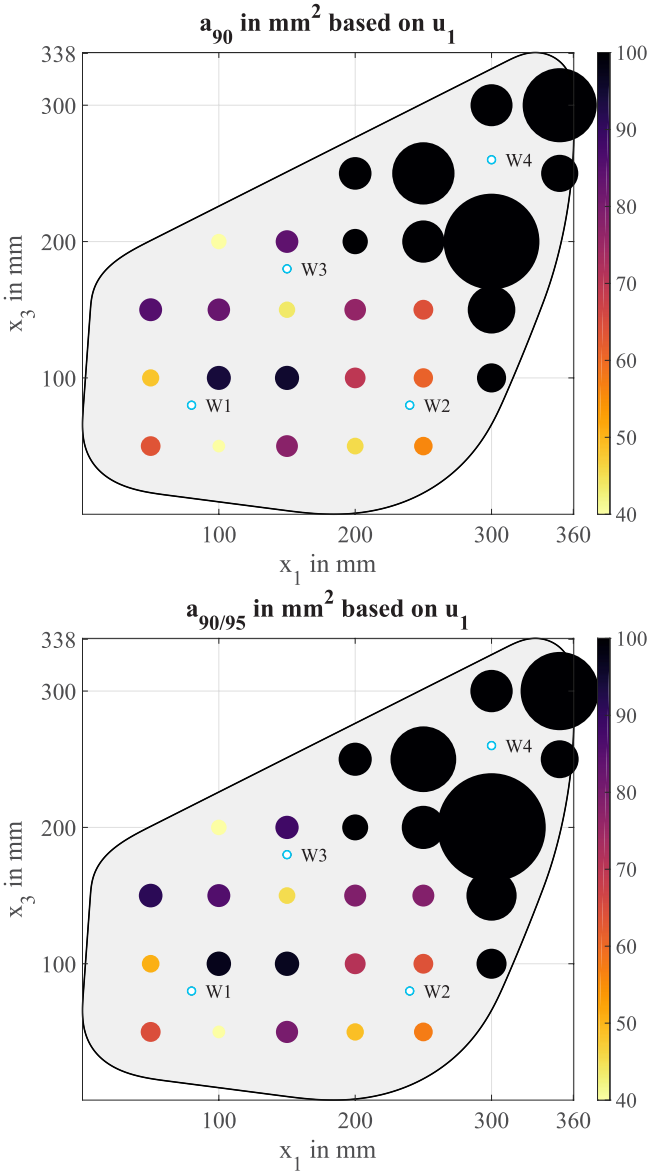

Fig. 9. Graphic representation of the determined a_{90} and $a_{90/95}$ values based on the evaluation of u_1. The transducer W1 was the actuator, the transducer W2 the sensor. Top: a_{90}. Bottom: $a_{90/95}$.

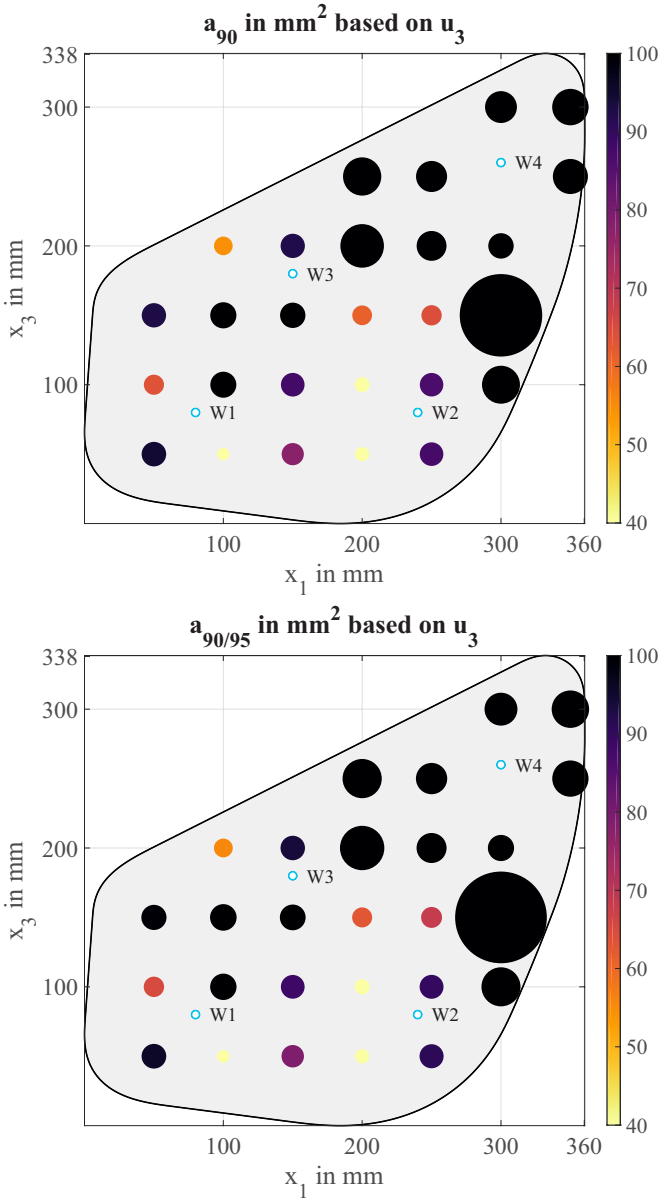

Fig. 10. Graphic representation of the determined a_{90} and $a_{90/95}$ values based on the evaluation of u_3. The transducer W1 was the actuator, the transducer W2 the sensor. Top: a_{90}. Bottom: $a_{90/95}$.

scattered wave component. However, this scattered wave only shows a clear influence on the u_1 differential signal at W2 at a high value of a. When evaluating the u_3 component, the determined a_{90} and $a_{90/95}$ values mostly decrease (Figure 10). Moreover, the acceptance criterion cannot be met for 3 damage positions within the region between W1, W2 and W3.

By interpolating the determined a_{90} and $a_{90/95}$ values from Figure 9 and 10 to a finer grid, a POD map could be generated, respectively. The finer grid was chosen with a resolution of $\Delta x = 0.5\,\text{mm}$. The Matlab function *scatteredInterpolant* was used with the natural neighbour interpolation [62]. The results are shown in Figure 11 and 12. These graphic representations once again illustrate the investigation of the actuator-sensor combination W1-W2 described above. The acceptance criterion can be met in the region between W1, W2 and W3, whereas this is not the case in the "Northeast" of the test specimen. When evaluating the u_1 time signals a maximum value of $a_{90/95} = 1910.58\,\text{mm}^2$ could be determined among all damaged positions; when evaluating the u_3 time signals a maximum value of $1318.38\,\text{mm}^2$ was determined.

In contrast, if the actuator-sensor combination W3-W4 is used, the POD maps change (Figures 13 and 14). In the region between W3 and W4, damage below the acceptance criterion of $100\,\text{mm}^2$ can now be detected. At the same time, this is not possible in areas in the "West", "South" and "East" of the test specimen, *i. e.* this actuator-sensor combination is also not suitable for globally meeting the acceptance criterion.

This article has been accepted for publication in a future issue of this journal, but has not been fully edited. Content may change prior to final publication. Citation information: DOI 10.1109/TUFFC.2021.3084898, IEEE Transactions on Ultrasonics, Ferroelectrics, and Frequency Control

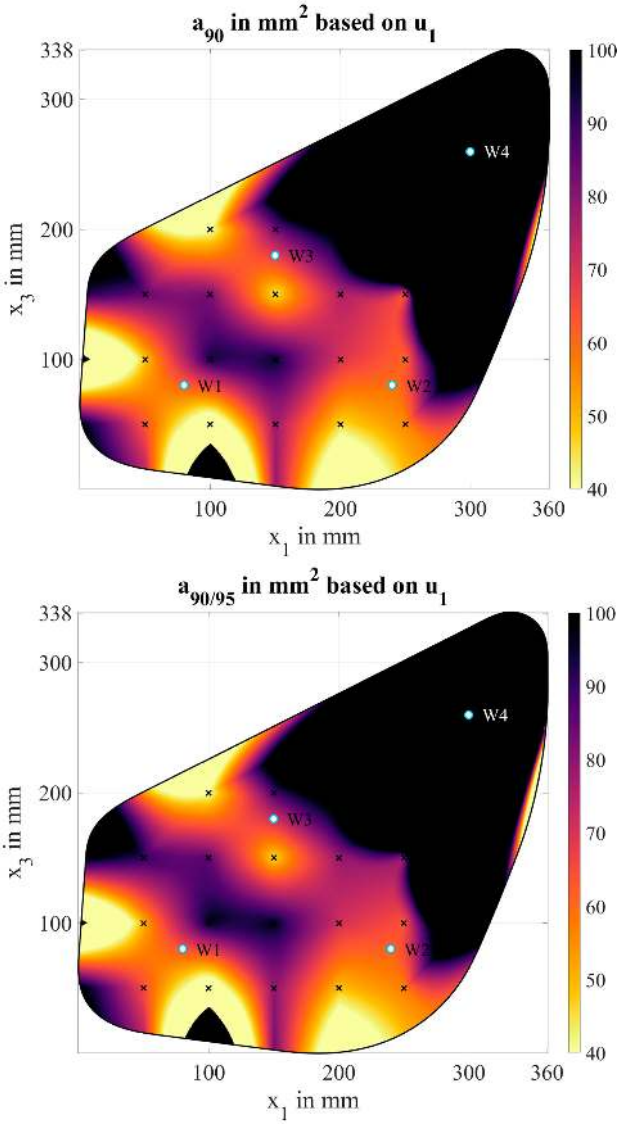

Fig. 11. The POD maps obtained by interpolation from Figure 9. The transducer W1 was the actuator, the transducer W2 the sensor. Top: a_{90}. Bottom: $a_{90/95}$.

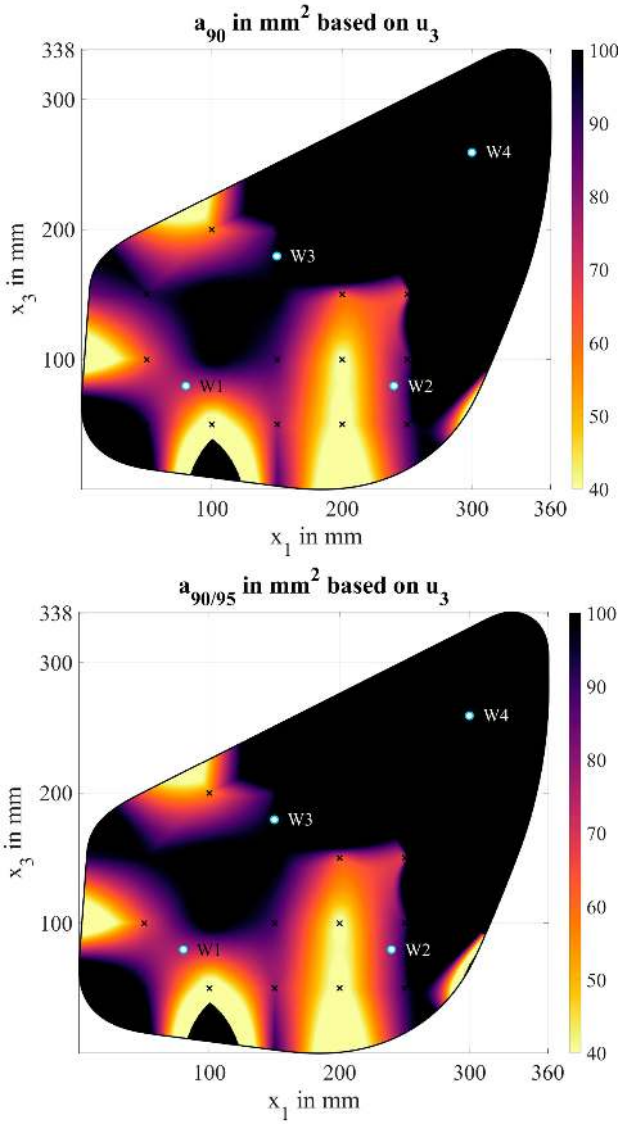

Fig. 12. The POD maps obtained by interpolation from Figure 10. The transducer W1 was the actuator, the transducer W2 the sensor. Top: a_{90}. Bottom: $a_{90/95}$.

Here, a local dependence of the POD is again confirmed. In general, the u_3 component of the displacement is more sensitive to a damage. On the one hand, when evaluating the u_3 component, the determined a_{90} and $a_{90/95}$ values are lower in the region between W3 and W4, on the other hand, the acceptance criterion can be met in two areas around W1 and W2 (Figure 14). By evaluating the u_1 time signals a maximum $a_{90/95}$ value of 333.28 mm^2 could be determined for the test specimen and, by evaluating the u_3 time signals, a maximum value of 252.33 mm^2.

D. Discussion

The preliminary investigations confirm that the POD within the SHM system depends on the arrangement of the transducers or the selected actuator-sensor combination. It follows that there is an optimal actuator-sensor combination for each damage position. In this context, optimal means that the actuator-sensor combination with the smallest a_{90} and $a_{90/95}$ value is selected. For example, the actuator-sensor combination W4-W1 was found to be optimal for the damage location at the position $x_1 = 100$ mm and $x_3 = 100$ mm with $a_{90} = 27.4$ mm^2 and $a_{90/95} = 29$ mm^2 when evaluating the u_1 component or $a_{90} = 30.62$ mm^2 and $a_{90/95} = 31.9$ mm^2 when evaluating the u_3 component. The order between the actuator and the sensor must be explicitly considered, since reciprocity on a Pitch-Catch path does not necessarily apply after a damage has been introduced due to anisotropy. For the entire system, therefore, not only an optimal actuator-sensor combination can be specified for each damage position, but also the component of the displacement that shows the higher interaction, *i. e.* the

This article has been accepted for publication in a future issue of this journal, but has not been fully edited. Content may change prior to final publication. Citation information: DOI 10.1109/TUFFC.2021.3084898, IEEE Transactions on Ultrasonics, Ferroelectrics, and Frequency Control

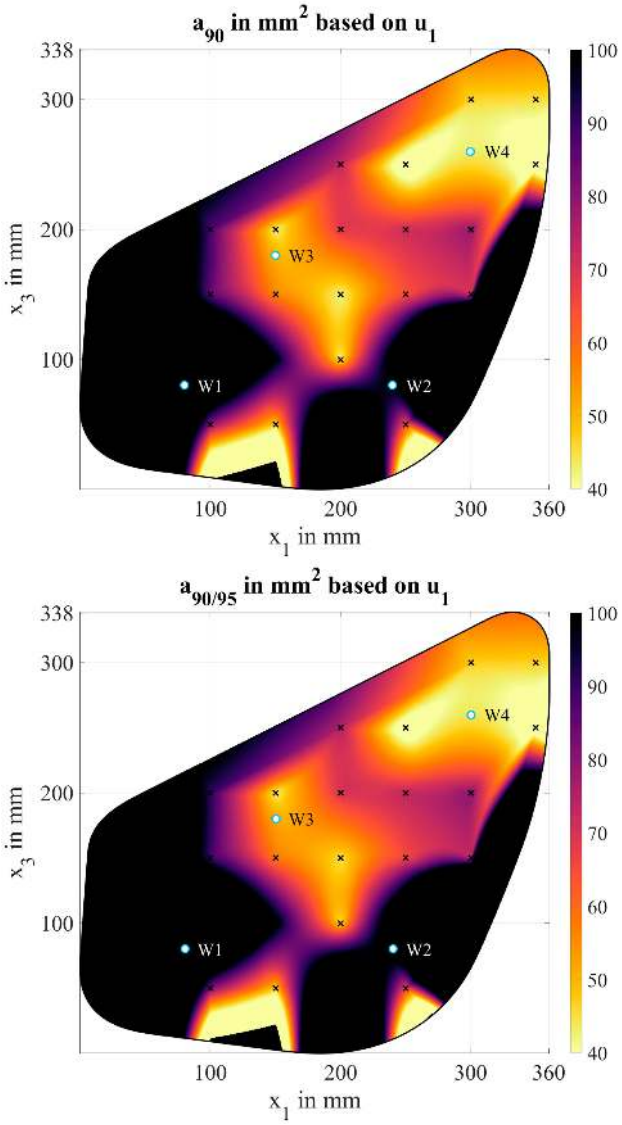

Fig. 13. The POD maps obtained by interpolation based on evaluation of u_1. The transducer W3 was the actuator, the transducer W4 the sensor. Top: a_{90}. Bottom: $a_{90/95}$.

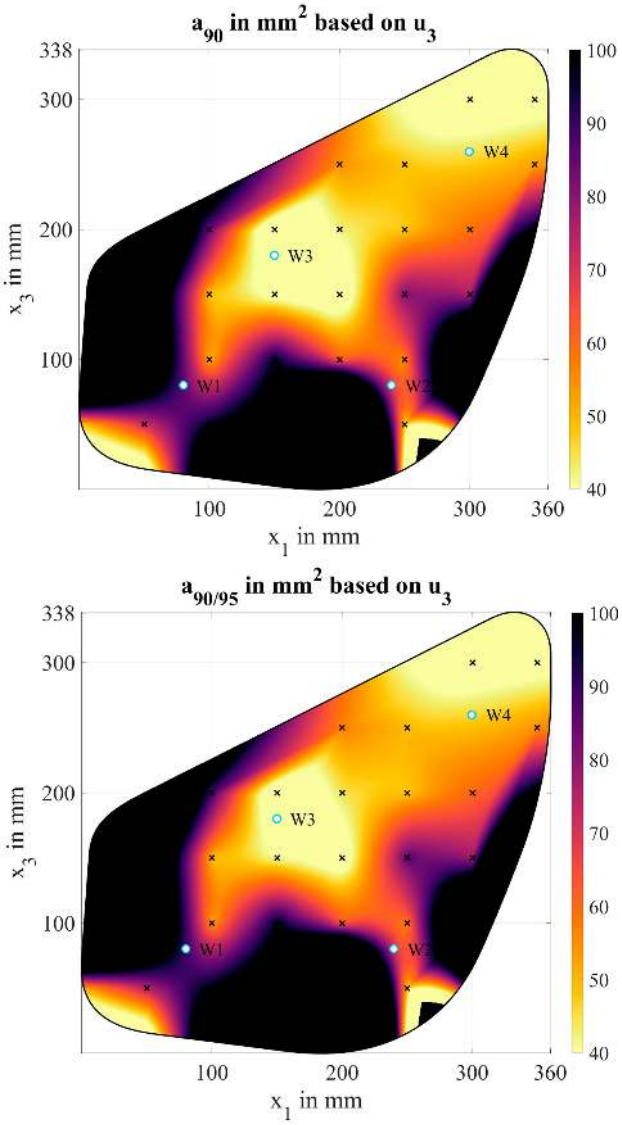

Fig. 14. The POD maps obtained by interpolation based on evaluation of u_3. The transducer W3 was the actuator, the transducer W4 the sensor. Top: a_{90}. Bottom: $a_{90/95}$.

component where a_{90} and $a_{90/95}$ is smaller. In the example above, this is the u_1 displacement with $a_{90} = 27.4\,\mathrm{mm}^2$ and $a_{90/95} = 29\,\mathrm{mm}^2$.

Figure 15 shows the a_{90} and $a_{90/95}$ values that are selected as optimal for all damage positions, among all actuator-sensor combinations and between the components of the displacement. By interpolation of the determined a_{90} and $a_{90/95}$ values from Figure 15 the POD map of the entire SHM system can finally be obtained (Figure 16). It can be seen that the entire system can meet the acceptance criterion of $100\,\mathrm{mm}^2$, which does not apply to every actuator-sensor combination as one can see from the examples in Figures 11 to 14. The maximum $a_{90/95}$ value of $75.59\,\mathrm{mm}^2$ could be determined for the whole CFRP component. In a region in the "Northwest" of the test specimen and at $x_1 = 150\,\mathrm{mm}$ and $x_3 = 100\,\mathrm{mm}$ only defects of the certain sizes can be detected with the needed probability and other smaller damage will be missed. This result is particularly pronounced for the latter damage position, as it is located in a region between W1, W2 and W3, and is, nevertheless, difficult to detect. Due to the anisotropy of the specimen and the resulting characteristic of the wave propagation, it follows that the scattered wave field of this damaged area predominantly "passes" the transducers W1, W2 and W3 (Figure 5). Only a relatively large area of damage causes a reflected signal that is above the decision threshold.

The structure of the distribution of the a_{90} and $a_{90/95}$ values with regions of smaller and regions of higher values that directly adjoin one another was also observed in the literature. The authors of [60] visualised the maximum amplitude that can be achieved by constructive superposition of excited wave

This article has been accepted for publication in a future issue of this journal, but has not been fully edited. Content may change prior to final publication. Citation information: DOI 10.1109/TUFFC.2021.3084898, IEEE Transactions on Ultrasonics, Ferroelectrics, and Frequency Control

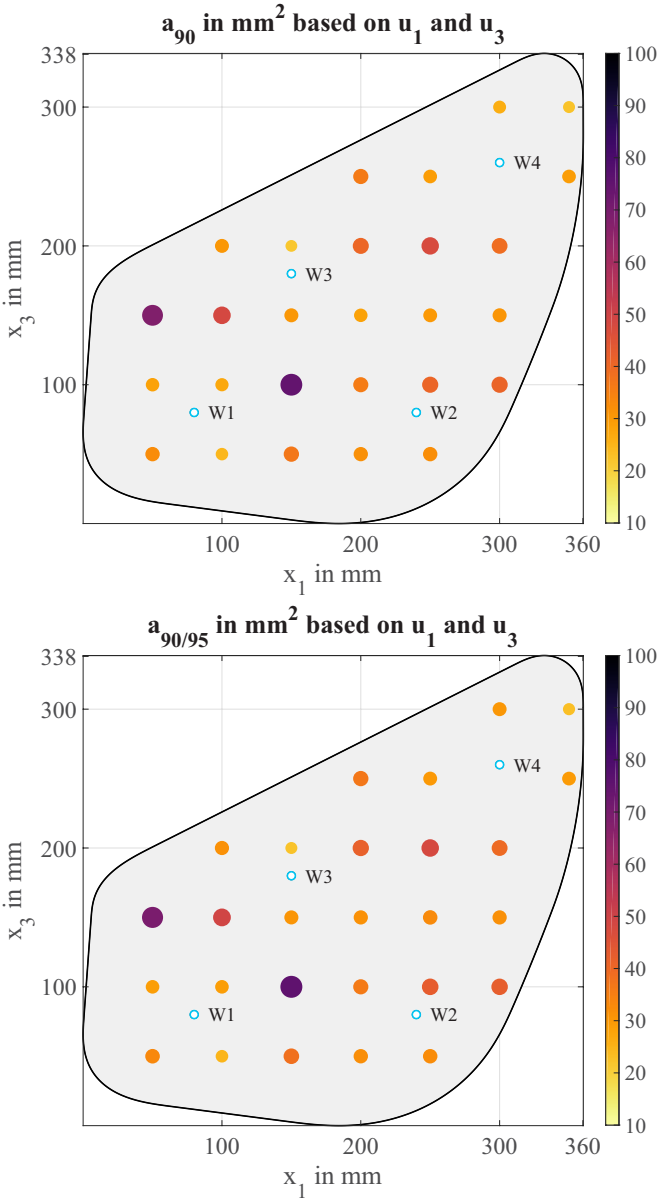

Fig. 15. Graphic representation of the lowest a_{90} and $a_{90/95}$ values at the current damage positions among all actuator-sensor combinations. Top: a_{90}. Bottom: $a_{90/95}$.

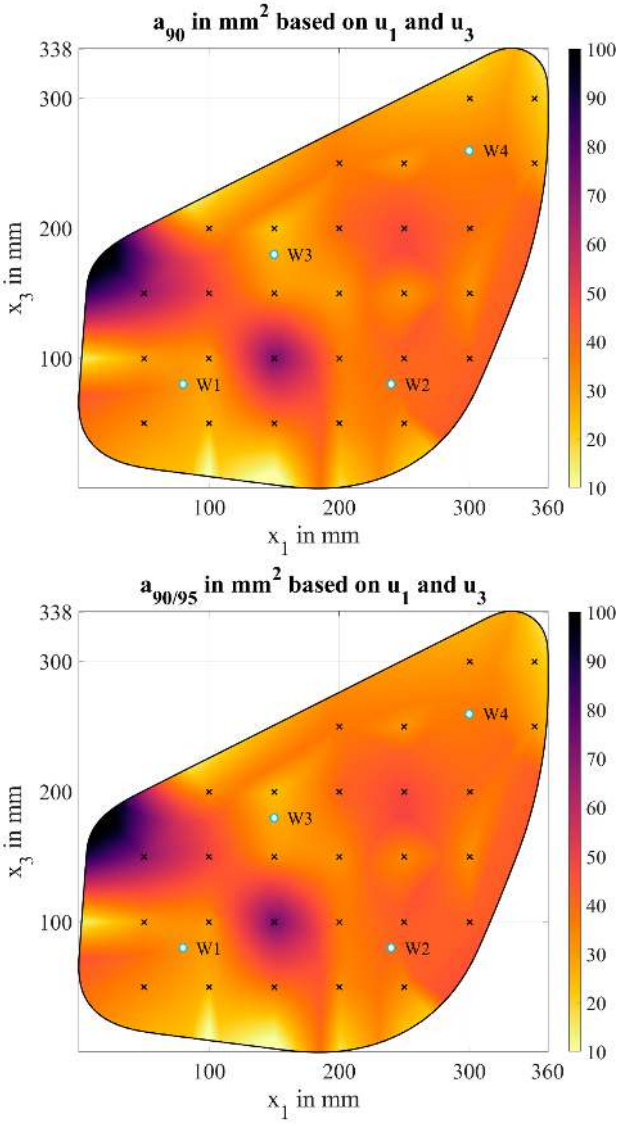

Fig. 16. The POD maps obtained by interpolation from Figure 15. Top: a_{90}. Bottom: $a_{90/95}$.

modes in a metal plate depending on the location. This maximum amplitude is directly related to a possible interaction with a damaged area and thus to the damage sizes that can be detected depending on the location. For anisotropic, plate-like structures made of fibre composite materials, the authors in [10], [34] show examples of imaging techniques used for damage detection. These examples also show that areas of high interaction can be located directly next to regions of less interaction. The causes are different distances between actuator, sensor and damage position as well as the anisotropic structure of the test object. Due to the purely model-based approach, the absolute values of POD curves and POD maps cannot be easily transferred to experimental investigations. On the one hand the determination of a decision threshold was realised using insensitive paths at the smallest modelled damage. Measurement noise was not taken into account due to the nature of simulation. On the other hand, other influencing parameters like temperature variation or variation of stresses have also not been included in the analysis. Moreover the transducer itself has not been modelled. Instead, the resulting u_1 and u_3 components have been analysed. Nevertheless, the qualitative statements of the study enable a highly improved knowledge about the system performance. Especially the POD map allows for a location specific analysis of the system performance and enables SHM system engineers to make informed decisions during design and operation phase.

V. Conclusion

In the present work, the Elastodynamic Finite Inetgration Technique was used to model a curvilinear automotive component made of carbon fibre reinforced plastics. Furthermore, the Equivalent Single Layer approach was used in the context of the discretisation scheme to model the anisotropic material behaviour of multi-layered composites. These developments were then combined in order to check the feasibility of the Model-Assisted Probability of Detection (MAPOD) principle on the exemplary modelled automotive component. The approach for generating POD curves was taken from classical non-destructive testing and transferred to the modelled Structural Health Monitoring (SHM) system. To characterise the performance of the SHM system, a method for creating POD maps was presented and implemented. The results obtained visualise whether the SHM system is able to hold the acceptance criterion defined for the investigation. Nevertheless, a continuing comparison of the model and experimental data is still necessary to provide a complete reliability assessment of the SHM systems. The developments of the present work can be used as tools for the model-assisted evaluation and optimisation of an SHM system.

Acknowledgment

Parts of this work were funded by the German Federal Ministry of Education and Research in the project "Carbon-Safe" (funding code: 16ES0333). The collaboration of the authors was supported by the DFG within the project "Towards a holistic quality assessment for guided wave based SHM" (project number 424954879).

References

[1] P. Cawley, "Structural health monitoring: Closing the gap between research and industrial deployment," *Structural Health Monitoring*, vol. 17, pp. 1225–1244, 2018.

[2] J. C. Aldrin, E. A. Medina, E. A. Lindgren, C. F. Buynak, and J. Knopp, "Protocol for Reliability Assessment of Structural Health Monitoring Systems Incorporating Model-assisted Probability of Detection (MAPOD) Approach," tech. rep., Air Force Research Laboratory, 2011.

[3] K. V. Jata, J. Knopp, J. C. Aldrin, and E. A. Medina, "Transitioning from NDE Inspection to Online Structural Health Monitoring - Issues and Challenges," in *Proceedings of the Third European Workshop on Structural Health Monitoring* (A. Güemes, ed.), 2006.

[4] A. Gianneo, M. Carboni, and M. Giglio, "Feasibility study of a multi-parameter probability of detection formulation for a Lamb waves-based structural health monitoring approach to light alloy aeronautical plates," *Structural Health Monitoring*, vol. 16, no. 2, pp. 225–249, 2017.

[5] J. L. Rose, "A Baseline and Vision of Ultrasonic Guided Wave Inspection Potential," *Journal of Pressure Vessel Technology*, vol. 124, pp. 273–282, 2002.

[6] L. Schubert, U. Lieske, B. Köhler, and B. Frankenstein, "Interaction of Lamb Waves with impact damaged CFRP's studied by Laser-Vibrometry and Acousto Ultrasonic," in *18th European Conference on Fracture*, (Dresden), 2010.

[7] L. Schubert, U. Lieske, B. Frankenstein, and B. Köhler, "Interaction of Lamb waves with impact damaged CFRP's - effects and conclusions for acousto-ultrasonic applications," in *Proceedings of the 7th International Workshop on Structural Health Monitoring*, pp. 151–158, 2009.

[8] V. Giurgiutiu, *Structural Health Monitoring with piezoelectric wafer active sensors*. Academic Press, 2008.

[9] E. Monaco, V. Memmolo, F. Ricci, and L. Maio, "Guided waves based SHM systems for composites structural elements: statistical analyses finalized at propability of detection and assessment," in *Health Monitoring of Structural and Biological Systems*, vol. 9438, Proceedings SPIE, 2015.

[10] R. Loendersloot, I. Buethe, P. Michaelides, M. Moix-Bonet, and G. Lampeas, "Damage Identification in Composite Panels - Methodologies and Visualisation," in *Smart Intelligent Aircraft Structures (SARISTU)*, pp. 579–604, 2016.

[11] R. Loendersloot and M. Moix-Bonet, "Damage Identification in Composite Panels using Guided Waves," in *5th CEAS Air & Space Conference*, 2015.

[12] M. Moix-Bonet, B. Eckstein, R. Loendersloot, and P. Wierach, "Identification of Barely Visible Impact Damage on a Stiffened Composite Panel with a Probability-based Approach," in *10th International Workshop on Structural Health Monitoring*, 2015.

[13] M. Moix-Bonet, P. Wierach, R. Loendersloot, and M. Bach, "Damage Assessment in Composite Structures Based on Acousto-Ultrasonics - Evaluation of Performance," in *Smart Intelligent Aircraft Structures (SARISTU)*, pp. 617–629, 2016.

[14] I. Mueller, *Inspection of Piezoelectric Transducers used for Structural Health Monitoring Systems*. Dissertation, Universität Siegen, 2017. Schriftreihe der Arbeitsgruppe für Technische Mechanik im Institut für Mechanik und Regelungstechnik - Mechatronik.

[15] C. A. Harding and G. R. Hugo, "Statistical Analysis of Probability of Detection Hit/Miss Data for small Data Sets," *Review of Quantitative Nondestructive Evaluation*, vol. 22, pp. 1838–1845, 2003.

[16] C. A. C. Leckey, M. D. Rogge, and F. R. Parker, "Guided waves in anisotropic and quasi-isotropic aerospace composites: Three-dimensional simulation and experiment," *Ultrasonics*, vol. 54, pp. 385–394, 2014.

[17] SAE, "SAE International Deutschland." http://de.sae.org, 2019. Last call: 2019.11.12.

[18] H. Gravenkamp, A. A. Saputra, C. Song, and C. Birk, "Efficient wave propagation simulation on quadtree meshes using SBFEM with reduced modal basis," *International Journal for Numerical Methods in Engineering*, vol. 110, pp. 1119–1141, 2016.

[19] I. Buethe, N. Dominguez, H. Jung, C.-P. Fritzen, D. Ségur, and F. Reverdy, "Path-Based MAPOD Using Numerical Simulations," in *Smart Intelligent Aircraft Structures (SARISTU)*, pp. 631–642, 2016.

[20] G. A. Georgiou, "Probability of Detection (PoD) curves," tech. rep., Jacobi Consulting Limited, London, 2006.

[21] L. Le Gratiet, B. Iooss, G. Blatman, T. Browne, S. Cordeiro, and B. Goursaud, "Model Assisted Probability of Detection curves: New statistical tools and progressive methodology," *HAL - archives ouvertes*, 2016.

[22] R. M. Meyer, J. P. Lareau, S. L. Crawford, and M. T. Anderson, "Review of Literature for Model Assisted Probability of Detection," tech. rep., Pacific Northwest National Laboratory, 2014.

[23] A. P. Berens, *ASM Metals Handbook: Nondestructive Evaluation and Quality Control*, vol. 17, ch. NDE Reliability Data Analysis, pp. 689–701. ASM International, 1988.

[24] M. Pavlovic, K. Takahashi, C. Müller, and R. Boehm, "NDT Reliability - Final Report: Reliability in non-destructive testing (NDT) of the canister components," tech. rep., BAM - Federal Institute for Materials Research and Testing, 2008.

[25] S. Kessler and G. Jarmer, "Probability of Detection Assessment of a Guided Wave Structural Health Monitoring System," in *Proceedings of the 10th International Workshop on Structural Health Monitoring*, 2015.

[26] A. P. Berens, "Probability of Detection (POD) Analysis for the Advanced Retirement for Cause (RFC)/Engine Structural Integrity Program (ENSIP) Nondestructive Evaluation (NDE) System Development, Volume 1 - POD Analysis," tech. rep., University of Dayton, 2000.

[27] A. Gallina, P. Packo, and L. Ambroziński, *Advanced Structural Damage Detection: From Theory to Engineering Application*, ch. Model Assisted Probability of Detection in Structural Health Monitoring, pp. 57–72. John Wiley & Sons Ltd., 2013.

[28] MIL-HDBK, "Nondestructive Evaluation System Reliability Assessment." United States of America, Department of Defense Handbook, 2009.

[29] A. P. Berens and J. S. Loomis, "Probability of Detection (POD) Analysis for the Advanced Retirement for Cause (RFC)/Engine Structural Integrity Program (ENSIP) Nondestructive Evaluation (NDE) System Development, Volume 2 - Users Manual," tech. rep., University of Dayton, 2000.

[30] A. P. Berens, W. Hoppe, D. A. Stubbs, and O. Scott, "Probability of Detection (POD) Analysis for the Advanced Retirement for Cause (RFC)/Engine Structural Integrity Program (ENSIP) Nondestructive

Evaluation (NDE) System Development, Volume 3 - Material Correlation Study," tech. rep., University of Dayton, 2000.

[31] L. Gandossi and C. Annis, "Probability of Detection Curves: Statistical Best-Practices," tech. rep., European Network for Inspection and Qualification, 2010. ENIQ Report 41.

[32] D. S. Forsyth and J. C. Aldrin, "Build your own POD," in *4th European-American Workshop on Reliability of NDE, Berlin*, 2009.

[33] L. Schaefer, "Tutorial: POD Basic," in *4th European-American Workshop on Reliability of NDE*, (Berlin), 2009.

[34] V. Memmolo, F. Ricci, L. Maio, N. D. Boffa, and E. Monaco, "Model assisted probability of detection for a guided waves based SHM technique," in *SPIE Smart Structures and Materials + Nondestructive Evaluation and Health Monitoring*, 2016.

[35] Z. Su and L. Ye, *Identification of Damage Using Lamb Waves - From Fundamentals to Applications*, vol. 48 of *Lecture Notes in Applied and Computational Mechanics*. Springer-Verlag Berlin Heidelberg, 2009.

[36] V. Memmolo, N. Boffa, L. Maio, E. Monaco, and F. Ricci, "Damage localization in composite structures using a guided waves based multi-parameter approach," *Aerospace*, vol. 5, no. 4, 2018.

[37] N. Nakagawa and R. B. Thompson, "Modelling ii model-assisted probability of detection : Use of nde models and statistical qualification of model predictions," in *7th International Conference on NDE in Relation to Structural Integrity for Nuclear and Pressurized Components*, 2010.

[38] T. Sollier and C. Blain, "IRSN preliminary analysis on statistical methods for NDE performance assessment," in *12th International Conference on Non Destructive Evaluation in Relation to Structural Integrity for Nuclear and Pressurized Components*, (Dubrovnik), 2016.

[39] C. Mueller, M. Bertovic, D. Kanzler, and U. Ronneteg, "Conclusions of the 6th european american workshop on reliability of nde," vol. 1706, 2016.

[40] A. C. Cobb, J. Fisher, and J. E. Michaels, "Model-Assisted Probability of Detection for Ultrasonic Structural Health Monitoring," in *4th European-American Workshop on Reliability of NDE*, (Berlin), 2009.

[41] C. Harding, G. Hugo, and S. Bowles, "Model-Assisted Probability of Detection Validation of Automated Ultrasonic Scanning for Crack Detection at Fastener Holes," in *10th Joint Conference on Aging Aircraft*, 2007.

[42] P. Fellinger, R. Marklein, K.-J. Langenberg, and S. Klaholz, "Numerical modeling of elastic wave propagation and scattering with EFIT - elastodynamic finite integration technique," *Wave Motion*, vol. 21, pp. 47–66, 1995.

[43] F. Schubert, A. Pfeiffer, B. Köhler, and T. Sanderson, "The elastodynamic finite integration technique for waves in cylindrical geometries," *The Journal of the Acoustical Society of America*, vol. 104, pp. 2604–2614, 1998.

[44] F. Schubert, "Numerical time-domain modeling of linear and nonlinear ultrasonic wave propagation using finite integration technique - theory and applications," *Ultrasonics*, vol. 42, pp. 221–229, 2004.

[45] K. Tschöke and H. Gravenkamp, "On the numerical convergence and performance of different spatial discretization techniques for transient elastodynamic wave propagation problems," *Wave Motion*, vol. 82, pp. 62–85, 2018. Submitted for publication.

[46] A. R. Levander, "Fourth-order finite-difference P-SV seismograms," *Geophysics*, vol. 53, no. 11, pp. 1425–1436, 1988.

[47] P. Moczo, J. O. A. Robertsson, and L. Eisner, "The Finite-Difference Time-Domain Method for Modeling of Seismic Wave Propagation," *Advances in Geophysics*, vol. 48, pp. 421–516, 2007.

[48] J. O. A. Robertsson, R. Laws, C. Chapman, J.-P. Vilotte, and E. Delavaud, "Modelling of scattering of seismic waves from a corrugated rough sea surface: a comparison of three methods," *Geophysical Journal International*, vol. 167, pp. 70–76, 2006.

[49] T. Gaul, K. Tschöke, E. Schulze, and L. Schubert, "Development and evaluation of Structural Health Monitoring systems for fibre composites in automotive application based on elastic waves," in *9th European Workshop on Structural Health Monitoring*, (Manchester), 2018.

[50] K. Tschöke, T. Gaul, B. Weihnacht, and L. Schubert, "Modelling Composites for Structural Health Monitoring Systems using Acoustic Ultrasonic Methods," in *8th KMM-VIN Industrial Workshop - Modelling of Composite Materials and Composite Coatings*, 2018.

[51] K. Tschöke, T. Gaul, T. Klesse, U. Lieske, F. von Dungern, J. Guerrero-Santafe, and H. Wessel-Segebade, "Development of an integrated measurement system for CFRP components within automotive manufacture," in *Proceedings of 47th National Conference on Nondestructive Testing (KKBN)*, 2018.

[52] L. Maio, V. Memmolo, F. Ricci, N. D. Boffa, E. Monaco, and R. Pecora, "Ultrasonic wave propagation in composite laminates by numerical simulation," *Composite Structures*, vol. 121, pp. 64–74, 2015.

[53] W. Van Paepegem and J. Degrieck, "Modelling Strategies for Fatigue Damage Behaviour of Fibre-reinforced Polymer Composites," *European Journal of Mechanical and Environmental Engineering*, vol. 46, no. 4, pp. 217–227, 2001.

[54] A. Karmazin, *Time-efficient Simulation of Surface-excited Guided Lamb Wave Propagation in Composites*. Dissertation, Karlsruher Institut für Technologie, Fakultät für Maschinenbau, 2012.

[55] R. Glüge and J. Kalisch, "The effective stiffness and stress concentrations of a multi-layer laminate," *Composite Structures*, vol. 111, pp. 580–586, 2014.

[56] eLamX, "Laminatberechnungsprogramm." Technische Universität Dresden, Institut für Luft- und Raumfahrttechnik, https://tu-dresden.de/ing/maschinenwesen/ilr/lft/elamx2/elamx, 2018. 12.07.2018.

[57] S.-Y. Lee, G. Rus, and T. Park, "Detection of stiffness degradation in laminate composite plates by filtered noisy impact testing," *Computational Mechanics*, vol. 41, no. 1, pp. 1–15, 2007.

[58] V. Dayal, V. Iyer, and V. K. Kinra, "Ultrasonic Evaluation of Microcracks in Composites," in *Advances in Fracture Research*, vol. 5, (Houston), pp. 3291–3300, 1989. Proceedings of the 7th International Conference on Fracture.

[59] SARISTU, "Smart Intelligent Aircraft Structures." http://www.saristu.eu/, 2017. 01.08.2017.

[60] F. Schubert, B. Frankenstein, M. Röllig, L. Schubert, and G. Lautenschläger, "Characterizing the Performance of Lamb Wave Based SHM Systems - A Two-Step Approach Based on Simulation-Supported POD and Reliability Aspects," in *5th European-American Workshop on Reliability of NDE*, (Berlin), 2013.

[61] R. S. Venkat, C. Boller, N. B. Ravi, N. Chakraborty, G. S. Kamalakar, K. Ukirde, and D. R. Mahapatra, "Optimized Actuator/Sensor Combinations for Structural Health Monitoring: Simulation and Experimental Validation," in *International Workshop on Strucutral Health Monitoring*, 2015.

[62] MathWorks, "Matlab Homepage." https://de.mathworks.com/help/matlab/ref/scatteredinterpolant.html, 2018. 14.07.2018.